BJR https://doi.org/10.1259/bjr.20211232

Received: 08 November 2021 | Accepted: 25 August 2022 | Published online: 11 October 2022

Cite this article as:
Henssen D, Meijer F, Verburg FA, Smits M. Challenges and opportunities for advanced neuroimaging of glioblastoma. *Br J Radiol* (2023) 10.1259/bjr.20211232.

REVIEW ARTICLE

Challenges and opportunities for advanced neuroimaging of glioblastoma

[1]DYLAN HENSSEN, [1]FREDERICK MEIJER, [2,3]FREDERIK A. VERBURG and [2,3]MARION SMITS

[1]Department of Medical Imaging, Radboud university medical center, Nijmegen, The Netherlands
[2]Department of Radiology & Nuclear Medicine, Erasmus MC, University Medical Centre Rotterdam, Rotterdam, The Netherlands
[3]Brain Tumour Centre, Erasmus MC Cancer Institute, Rotterdam, The Netherlands

Address correspondence to: Dr Dylan Henssen
E-mail: *dylan.henssen@radboudumc.nl*

ABSTRACT

Glioblastoma is the most aggressive of glial tumours in adults. On conventional magnetic resonance (MR) imaging, these tumours are observed as irregular enhancing lesions with areas of infiltrating tumour and cortical expansion. More advanced imaging techniques including diffusion-weighted MRI, perfusion-weighted MRI, MR spectroscopy and positron emission tomography (PET) imaging have found widespread application to diagnostic challenges in the setting of first diagnosis, treatment planning and follow-up. This review aims to educate readers with regard to the strengths and weaknesses of the clinical application of these imaging techniques. For example, this review shows that the (semi) quantitative analysis of the mentioned advanced imaging tools was found useful for assessing tumour aggressiveness and tumour extent, and aids in the differentiation of tumour progression from treatment-related effects. Although these techniques may aid in the diagnostic work-up and (post-)treatment phase of glioblastoma, so far no unequivocal imaging strategy is available. Furthermore, the use and further development of artificial intelligence (AI)-based tools could greatly enhance neuroradiological practice by automating labour-intensive tasks such as tumour measurements, and by providing additional diagnostic information such as prediction of tumour genotype. Nevertheless, due to the fact that advanced imaging and AI-diagnostics is not part of response assessment criteria, there is no harmonised guidance on their use, while at the same time the lack of standardisation severely hampers the definition of uniform guidelines.

INTRODUCTION

Glioblastoma (GBM) is the most common adult-type diffuse glioma, which arises from glial cells and concerns the most aggressive and malignant primary brain tumour with astrocyte-precursors, classified as Grade 4 by the World Health Organization (WHO) grading system. In spite of advances in treatment, the prognosis remains poor with a median survival of 14–16 months.[1,2] Following the recently published 2021 WHO Classification of Central Nervous System Tumours v. 5, GBM comprises only isocitrate dehydrogenase (*IDH*) wild-type tumours. All *IDH*-mutant diffuse astrocytic tumours are considered a single type called astrocytoma, *IDH*-mutant with WHO grades ranging from 2 to 4.[3] While the separation of astrocytomas into *IDH* wild-type and -mutated tumours is an important advance in GBM classification, all of the literature which is covered within this review is based on the 2016 WHO classification of central nervous system tumours[4] (or previous versions). Therefore, when the term GBM is utilised, this will not only include *IDH*-wildtype GBM; this will also comprise the new astrocytoma Grade 4 *IDH*-mutant entity.

Due to the continuous optimisation and development of imaging protocols, the role and value of neuroimaging in the diagnostic work-up and treatment evaluation of GBMs has increased over the last years. Advanced neuroimaging aids to non-invasively provide more certainty about the prognosis and response to therapy, which is beneficial for treatment decision-making and counselling of the patient. Therefore, the omnipresent role of advanced imaging in GBM is undisputed and further consolidation is driven by various major clinical and scientific societies (*e.g.* the European Society of Radiology, the Radiological Society of North America, the European Association of Nuclear Medicine, and the Society of Nuclear Medicine and Molecular Imaging).

The purpose of this review is to provide an educational overview of advanced neuroimaging techniques in GBM.

More specifically, advanced MRI techniques, including diffusion-weighted imaging (DWI), diffusion tensor imaging (DTI), perfusion-weighted imaging (PWI) techniques (both with and without the use of contrast-agents), and magnetic resonance spectroscopy (MRS), will be discussed. In addition, Fluorine-18 fludeoxyglucose (^{18}F-FDG-) and amino-acid tracer positron emission tomography (AA-PET) are discussed. We focus on the challenges and opportunities of applying these techniques in clinical practice. Also, some new developments within the field and the potential use of new radiotracers will be addressed. Furthermore, we discuss the potential added value of artificial intelligence (AI)-based tools. To conclude, we discuss possible solutions to avoid pitfalls in the study design, data acquisition, and data analyses for future clinical studies.

CONVENTIONAL MRI OF GLIOBLASTOMA

Brain MRI with conventional imaging sequences plays a pivotal role in the diagnosis and follow-up of glioblastoma. Traditionally, the conventional sequences used in neuro-oncology include T_1weighted (T_1W, T_2W, T_2W fluid attenuation inversion recovery (FLAIR), and post-contrast T_1W (T_1W + c) sequences.[5] Anatomical details of the brain and the neoplasm within can be accurately evaluated as well as peritumoral oedema and disruptions of the blood–brain barrier (BBB). Glioblastoma is characterised by a heterogeneous appearance on T_1W and T_2W, which can be explained by necrosis, haemorrhage, soft-tissue mass, and tumoural vasculature. The combination of an irregular enhancing lesion with areas of infiltrating tumour and cortical expansion is highly suggestive of GBM (Figure 1). However, the use of conventional MRI sequences alone limits the differentiation of GBM from other intracerebral mass lesions with cystic or necrotic components (*e.g.* other neuroglial tumours, brain metastasis, or brain abscess). In addition, conventional MRI is limited with regard to differentiating high from low-grade glioma.

In GBM, conventional MRI sequences provide some hallmark features which can aid to predict molecular markers. For example, small regions of enhancement, a larger non-enhancing tumour portion, well-defined tumour margins, and T_1W hypointense areas with suppressed FLAIR signal within its necrotic components are predictive of *IDH*1-mutation (Figure 2A).[6,7] In addition, a large volume of T_2W abnormality and a higher ratio of T_2W to T_1W + c tumour components were also found to be correlated with *IDH*-1 mutation (Figure 2B).[8] Tumour location of *IDH-1* mutation GBM in the frontal lobe has been reported most frequently by various groups.[9,10]

Next to *IDH*, the second most-reviewed gene is O^6-Methylguanine-DNA methyltransferase (*MGMT*). *MGMT* methylation status is another important biomarker because high activity of *MGMT* (*i.e.* unmethylated *MGMT*) is known to result in a reduced efficacy of alkylating chemotherapeutic agents (*e.g.* temozolomide). In high-grade gliomas such as GBM, *MGMT* methylation is less common as compared to low-grade gliomas.[11,12] On conventional MRI, hypermethylated *MGMT* tumours tend to have mixed-nodular enhancement in lesions which are non-temporally located (Figure 3A).[13] Unmethylated

Figure 1. Conventional imaging of glioblastoma. Exemplary axial (a) T_1 weighted images (with motion artefacts), (b) post-contrast T_1 weighted images (with motion artefacts), (c) T_2 weighted images and (d), FLAIR images. Contrast-enhancing lesion with non-enhancing components suggesting necrosis. The lesion is surrounded by T_2W/FLAIR hyperintense signal representing tumour infiltration and oedema. The lesion itself is observed to exert mass effect. FLAIR, fluid attenuated inversion recovery.

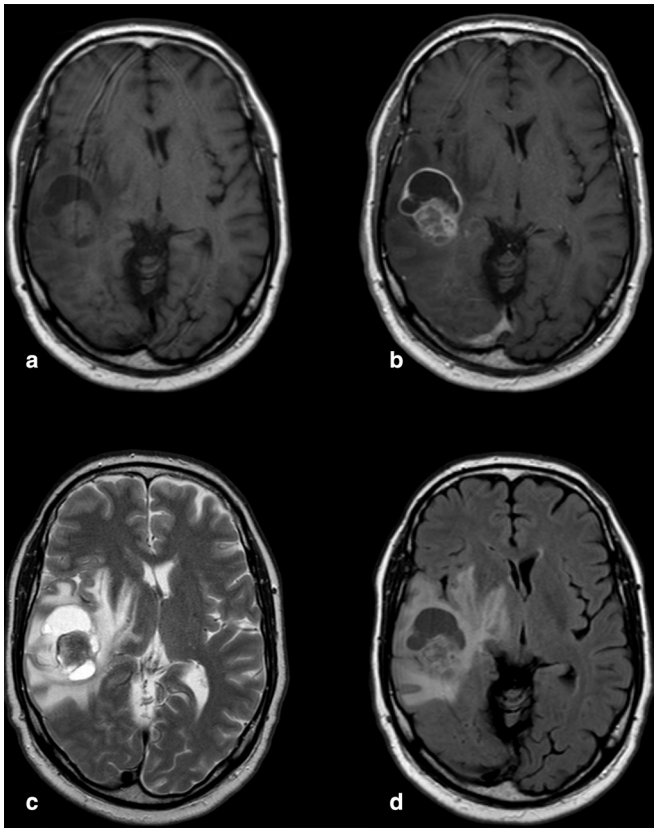

MGMT gliomas, on the other hand, show a ring-pattern enhancement (Figure 3B).[14]

In non-GBM, two radiological signs on conventional MRI sequences have been described in literature, which can provide insights in the mutational status. First, the T2-FLAIR mismatch sign describes that areas with T_2W-high signal intensity of the tumour are relatively hypointense in signal on T2-FLAIR images due to incomplete free water suppression. In addition, a rim of hyperintensity can be seen on FLAIR. These MRI features are considered a specific radiogenomic-signature of diffuse astrocytoma (*IDH*-mutant, 1p/19q intact) with a high positive predictive power.[15,16] The second radiogenomic-signature in non-GBM concerns the aspect of the T_2W-hyperintense signal and its delineation from the normal brain parenchyma. When this hyperintense area has smooth borders and has a homogeneous signal intensity, the tumour is more likely to be an astrocytoma without 1p/19q co-deletion.[17–19]

In the post-therapeutic setting, it has been advised to perform MRI within 2 days after surgical intervention to assess the extent

Figure 2. Conventional MRI of two patients, one with astrocytoma *IDH* mutant WHO Grade 4 and one with glioblastoma *IDH* wildtype. First row (a–d) shows an astrocytoma *IDH* mutant WHO Grade 4 located in the right frontal lobe with involvement of the rostrum corpus callosum. It is observed that only small regions of enhancing tumour are present on post-contrast T_1 weighted images (b; see arrow head in the enlarged section). On T_1 weighted images (a), very small hypointense areas which are also hypointense on FLAIR images (d) can be observed. Exemplary focus is encircled in the enlarged sections. These regions reflect necrotising/cystic regions. In addition, extensive T_2W hyperintense regions can be observed on T_2 weighted (c) and FLAIR images (d) surrounding the limited area of contrast-enhancing tumour. Second row (e–h) shows a glioblastoma *IDH* wildtype located in the left temporal lobe. It can be observed that a classical appearance is present with a relatively large ring-enhancing region on post-contrast T_1 weighted images (f). This contrast-enhancing tumour is surrounded by a similar amount of T_1W hyperintensity; see T_2 weighted images (g) and FLAIR images (h). FLAIR, fluid attenuated inversion recovery; IDH, isocitrate dehydrogenase.

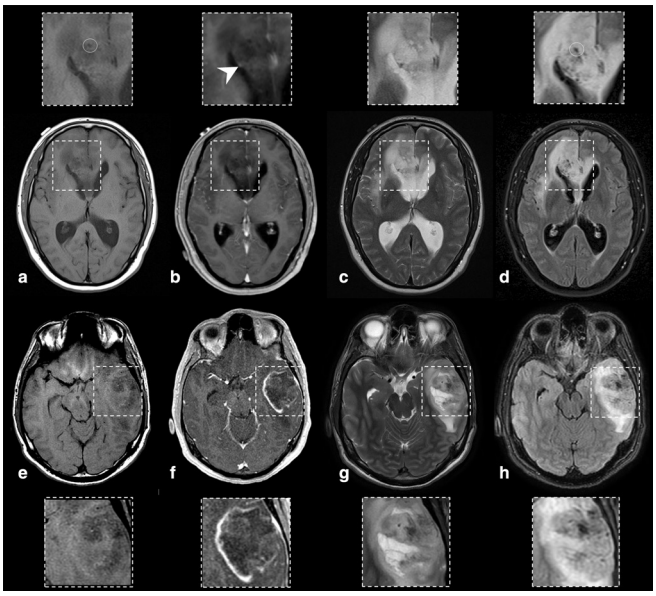

Figure 3. Axial post-contrast T_1 weighted images of patients suffering from glioblastoma with and without MGMT promoter methylation. (a) Axial post-contrast T_1 weighted images of three patients suffering from glioblastoma with MGMT promoter methylation showing a predominantly mixed-nodular pattern of enhancement. (b) Axial post-contrast T_1 weighted images of three patients suffering from glioblastoma without MGMT promoter methylation showing a predominantly ring-enhancement pattern. MGMT, O^6-Methylguanine-DNA methyltransferase.

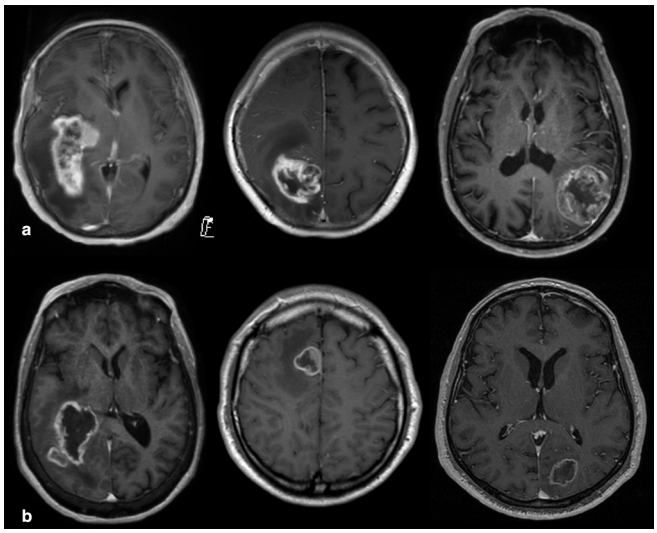

of the resection, the presence of residual tumour, and the occurrence of post-surgical complications.[20] In the post-operative setting, blood products in the resection cavity may be mistaken for residual enhancing lesion due to its intrinsic T1 shortening effects. Therefore, pre- and post-contrast T_1 weighted images must be evaluated with care. Nevertheless, enhancing lesions with a nodular aspect indicate residual neoplasm. Although these characteristics are generally reliable to assess residual or recurring neoplasm, some exceptions exist. Different treatment methods (*i.e.* chemotherapy and radiation) affect the permeability of the vascular walls which may lead to new enhancing lesions. If this contrast-enhancement is the result of treatment-induced vascular leakage, this is called pseudoprogression (PsP), whereas contrast-enhancement reflecting tumour recurrence is tumour progression (TP). Differentiation between PsP and TP is poor with conventional MR images alone (Figure 4). A 2011 study investigated the diagnostic accuracy of 11 signs as visible on conventional MRI to distinguish TP from PsP: 1) new enhancement; 2) marginal enhancement around the surgical cavity; 3) nodular enhancement; 4) callosal enhancement; 5) subependymal enhancement; 6) spreading wave front of enhancement; 7) cystic or necrotic change; 8) increased peritumoural T2 abnormality; 9) diffusion restriction; 10) decreasing enhancement intensity; and 11) increasing cystic or necrotic change. Only subependymal enhancement was found to have a limited predictive power with a sensitivity/specificity of 38/93% and with a negative-predictive value of 42%. The other 10 signs had no predictive power.[21]

DIFFUSION-WEIGHTED AND DIFFUSION-TENSOR MRI OF GLIOBLASTOMA

DWI is based on the random Brownian motion of water molecules and the magnitude of this Brownian motion is estimated as the apparent diffusion coefficient (ADC; mm^2/s). In turn, ADC is dependent on the cellular density and the presence of macromolecules or organelles/cell membranes in tissue compartments.[22] In gliomas, an inverse correlation between ADC values and tumour grade has been described.[23–25] DWI can also help to detect early tumour recurrence in enhancing and non-enhancing lesions seen as reduced diffusion[26] and to predict overall survival and progression-free survival in patients with glioblastoma.[27–30] DWI has been proposed to distinguish *MGMT* methylation status as a median ADC_{min} value of 800×10^{-6} mm^2/s or higher was found to represent methylated *MGMT* status.[31] DWI is, however, most commonly used to distinguish a brain abscess

Figure 4. Conventional MRI of two patients with glioblastoma in the post-treatment setting. Axial post-contrast T_1 weighted images of two patients with glioblastoma *IDH* wildtype. The upper images (a) show a region of contrast enhancement adjacent to the resection cavity in the right parietal lobe (white arrowheads). Radiological and clinical follow-up showed that this lesion represented pseudoprogression. The lower images (b) show nodular enhancement adjacent to the resection cavity in the left temporal lobe (white arrowheads). Radiological and clinical follow-up showed that this lesion represented tumour progression. IDH, isocitrate dehydrogenase.

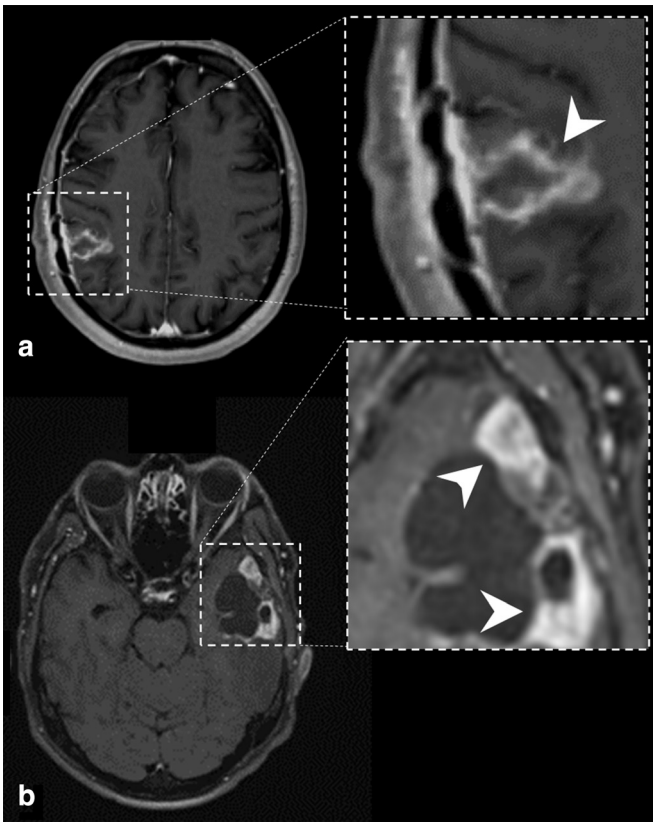

from glioma, and in the post-operative phase to identify areas of ischaemia.

In the post-therapeutic setting, differentiation between PsP and TP based on ADC values has been investigated by various groups (*e.g.*[32–42]). In general, it can be concluded that PsP lesions show a higher mean ADC-value as compared to the mean ADC-values in the TP group[26] (Figure 5). Although most studies on the use of ADC in the post-operative setting were conducted following a decent methodology, meta-analysis of ADC is hampered as different publications report different ADC metrics (*e.g.* mean, median, maximum, minimum). , When a quantitative assessment of ADC is carried out, it is recommended to use the mean ADC value of a region of interest (ROI), where necrotic areas should be excluded from the ROI-measurements. Reported cut-off values of mean ADC values to distinguish TP from PsP ranged between 1000×10^{-6} and 1412×10^{-6} mm^2/s corresponding with a range in sensitivity and specificity of 78–98.3% and 63.6–100% respectively.[43–46] The highest accuracy reported in

Figure 5. Diffusion-weighted imaging in tumour recurrence in a patient with glioblastoma. Axial post-contrast T_1 weighted images (a) show a new contrast-enhancing lesion cranial to the resection cavity in the right frontal lobe (white arrowheads). Restricted diffusion in this region is observed (white arrowheads) (b shows the corresponding ADC images; c shows the corresponding DWI images using a *b*-value of 1000 s/mm^2). This was highly suggestive for tumour progression, which was confirmed by radiological and clinical follow-up. ADC, apparent diffusion coefficient; DWI, diffusion-weighted imaging.

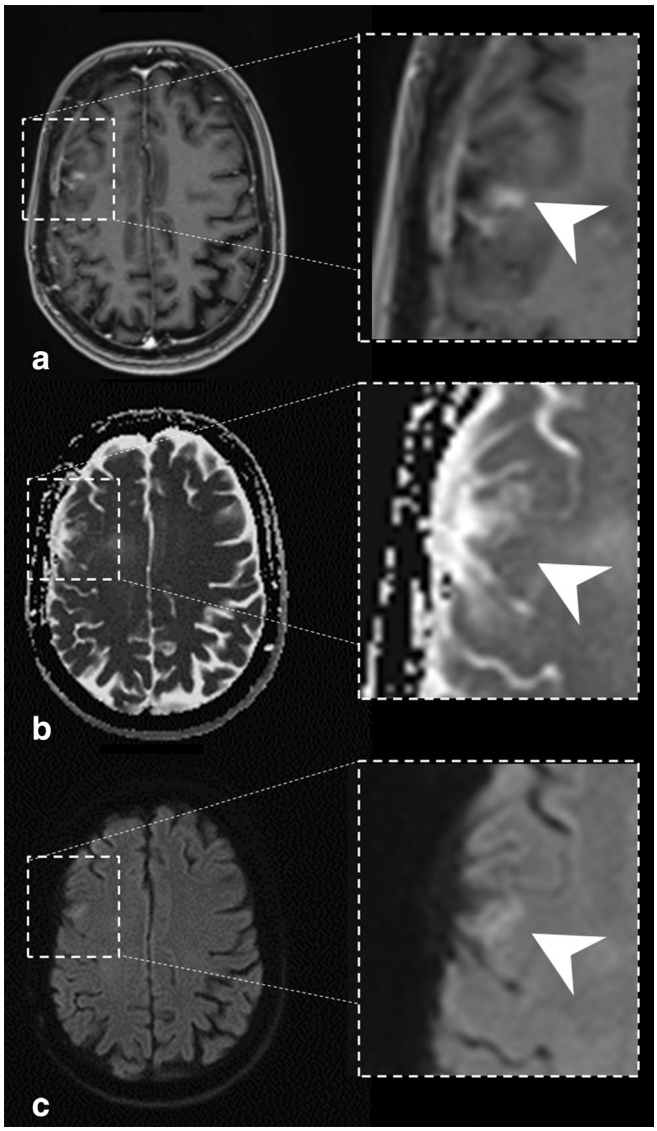

literature (sensitivity/specificity rate of 98.3/100%) was reported by using a cut-off value of mean ADC of 1313×10^{-6} mm^2/s to differentiate between PsP and TP with higher values reflecting TP.[44] It must be emphasised that ADC values in post-treatment gliomas depend on a variety of factors, including post-operative artefacts (*e.g.* pneumocranium) and MRI system-related specifications such as magnetic field strength and *b*-values.[37] Therefore, it is recommended to perform ROI-analysis on fixed locations at different time points, as this allows one to assess the longitudinal changes in ADC values.

DTI models complex tissue diffusivity, based on which the microstructural organisation of tissue can be evaluated. In DTI, additional gradient pulses are introduced which cause a random phase shift for diffusing molecules and cancel out stationary molecules.[47,48] In general, diffusion of water molecules in biological tissues tends to be anisotropic. The diffusion tensor can thus be represented by a diffusion ellipsoid with its main axis parallel to the principal diffusion direction within a voxel.[47,48] Different metrics can be derived from the DTI model (most used are mean diffusivity, MD and fractional anisotropy, FA). MD is comparable with ADC. FA serves as an index for the amount of diffusion anisotropy within the tissue; a value of 0 indicates isotropic water diffusion, whereas an FA value of 1 describes a maximally anisotropic voxel.[49] Some studies found that DTI metrics can be used to assess occult neoplastic invasion of white matter tracts[50,51] and the direction of tumour growth.[52] In clinical practice, DTI is mainly used for tractography to guide neurosurgical procedures.

In the post-therapeutic setting, FA-values were found useful to differentiate PsP from TP in various papers with low or moderate risk of bias; these papers showed higher FA-values in TP as compared to PsP.[42,53–55] However, no prospective studies on this topic were found. Reported cut-off values of mean FA values to distinguish TP from PsP ranged between 0.13 and 0.18 and corresponded with sensitivity and specificity values of 68–81% and 73–79% respectively.[46,54,56] The highest reported sensitivity/specificity (81/79%) was found with a cut-off FA-value of 0.18, with lower values reflecting TP.[54] However, interpreting the FA-values suffers from similar limitations as ADC value interpretation.

PERFUSION MRI OF GLIOBLASTOMA

The role of PWI of glioblastoma is mainly based on the presence of neovascularisation. Tumour neovascularisation concerns an extensive network of suboptimal, poorly organised vessels with slow flow and leakage.[57] On T_1W + c images, areas of contrast-enhancement are seen. Slow flow and other dynamic capacities of the neo-angiogenic network can be assessed by PWI. The most commonly used PWI techniques are dynamic susceptibility contrast (DSC) perfusion, dynamic contrast enhancement (DCE) perfusion, and arterial spin labelling (ASL).

DSC PWI relies on the susceptibility induced signal loss on T_2* weighted sequences, resulting from the passage of a bolus of gadolinium-based contrast agent. The most commonly used DSC perfusion parameter is cerebral blood volume (CBV) which can be estimated[58,59] and computed[60] based on the negative enhancement integral. Other parameters include cerebral blood flow (CBF), mean transit time (MTT) and time-to-peak (TTP). The estimated value of the area under the attenuation curve is proportional to the CBV but does not yield an absolute measurement. Therefore, the measurement is expressed relative to a standard reference, usually the contralateral white matter (relative CBV ratio: rCBV ratio).[61] Overall, the rCBV ratio is an indicator of hypervascular regions and serves as the most robust parameter in DSC imaging.[62]

DCE PWI relies on the evaluation of T1 shortening induced by a gadolinium-based contrast agent bolus leaking from the blood vessels in tissue. Pharmacokinetic modelling is used to derive various perfusion metrics including K^{trans}, V_e and V_p. K^{trans} represents the capillary permeability; V_e represents the fractional volume of the gadolinium-based contrast agent in the extravascular–extracellular space; V_p represents the fractional volume of the of the gadolinium-based contrast agent in the plasma space.[58]

Figure 6. Pre-operative MRI, including DSC perfusion weighted MRI, of glioblastoma. The upper row shows axial (a) T_2 weighted, (b) T_1 weighted and (c) post-contrast T_1 weighted images of a patient with *IDH* wildtype glioblastoma. The lower row shows two axial perfusion maps derived from DSC perfusion-weighted MRI, namely (d) CBV and (f) CBF. The area of T_1W-hyperintensity (presumably haemorrhage) shows low perfusion (white arrow heads), while the enhancing portion anterior to it shows increased perfusion (white arrows). CBF, cerebral blood flow; CBV, cerebral blood volume; DSC, dynamic susceptibility contrast; IDH, isocitrate dehydrogenase.

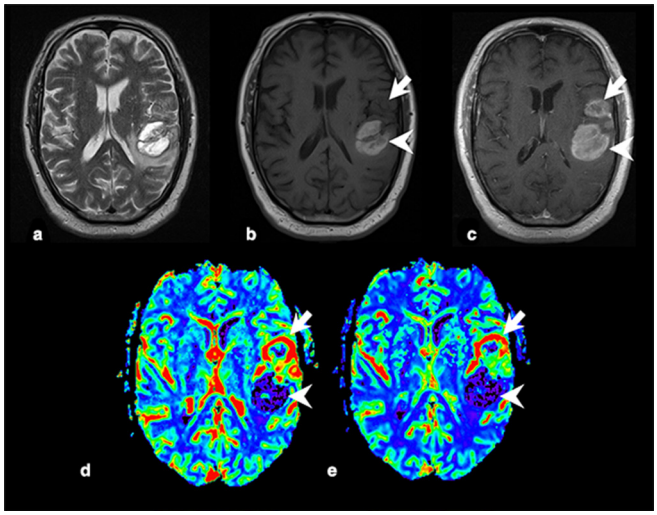

ASL is a perfusion technique without the need for contrast administration, where water molecules in blood vessels are tagged magnetically prior to entering the studied ROI (*i.e.* at the cervical level of the carotid artery). After a limited time interval (1.5–2.0 s), the labelled water molecules are imaged in the region of interest (*i.e.* the brain tissue). CBF values can be calculated from the differences in signal between the labelled images and the non-labelled images.[63,64] The major advantage of ASL is the fact that it does not suffer from contrast leakage effects.[65]

In the diagnostic work-up, PWI is used for characterisation of glioma genotype, as it is known that genetic differences in glioma subtypes correlate with the glioma vasculature. An exemplary image of DSC PWI in the pre-operative setting is provided in Figure 6. A recent review and meta-analysis reported that DSC-derived CBV values were fairly accurate when predicting *IDH* genotype, with an area under the receiver operator curve (AUROC) of 0.83.[66] When reviewing DCE parameters an AUROC of 0.81, 0.84 and 0.78 were observed for K^{trans}, V_e and V_p, respectively. Insufficient data were available with regard to the non-invasive genotype prediction of GBM based on ASL

Figure 7. Tumour progression of glioblastoma in the left temporal lobe as appreciated on post-contrast T_1 weighted images and DSC perfusion-weighted MRI. Enhancing lesion in the left temporal lobe in a patient post-treatment which shows increased cerebral blood volume on DSC perfusion-weighted MRI (white arrowhead). These features are highly suggestive for tumour progression, which was confirmed by radiological and clinical follow-up. DSC, dynamic susceptibility contrast.

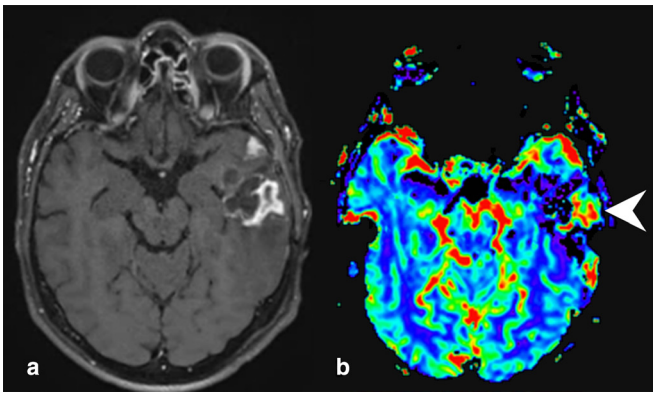

perfusion metrics. However, ASL could be used to differentiate between tumour grade (Grade 2, 3, 4) according to one meta-analysis.[67] Furthermore, some studies suggested that pre-treatment $rCBV_{max}$ values can be used as a prognostic marker for overall survival, or response to antiangiogenic treatment.[68–71]

Most commonly, PWI is used in the post-therapeutic setting to aid in the differentiation between TP and PsP. A recent meta-analysis on this topic reported the diagnostic accuracy of two DSC parameters: mean rCBV and maximum rCBV. Pooled sensitivity and specificity for detecting TP were both 88% for a $rCBV_{mean}$ ratio threshold ranging from 0.9 to 2.15. When using $rCBV_{max}$ ratios, pooled sensitivity and specificity for detecting TP were 93 and 76%, with thresholds derived from literature ranging from 1.5 to 3.1.[72] However, only the minority of papers included in these meta-analysis concerned prospective studies. An exemplary image of TP as assessed by DSC is shown in Figure 7.

Regarding the use of DCE-PWI to differentiate TP from PsP, two recent meta-analyses reported a pooled sensitivity ranging from 89 to 92%. In both meta-analyses, the specificity was found to be 85%,.[72,73] However, only the minority of papers included in these meta-analyses concerned prospective studies. Additionally, pooled diagnostic accuracies were not based on one DCE parameter but considered overall reported diagnostic accuracy of DCE. Contrary to specific meta-analyses on DSC parameters, no meta-analysis has been performed on the diagnostic accuracy of either K^{trans}, V_e or V_p in DCE PWI post-therapeutic glioblastoma. Therefore, no range of thresholds can be provided.

The use of ASL to differentiate PsP from TP has been suggested to be less accurate in comparison to other PWI techniques according to a recent meta-analysis.[73] This meta-analysis reported a sensitivity ranging between 52 and 79% and a specificity ranging between 64 and 82% when ALS was used to differentiate PsP from TP. However, too few studies are available to perform a proper meta-analysis with pooled sensitivities and specificities and further investigation is warranted. However, a recent paper from our group reports that ASL and DSC have similar diagnostic accuracies suggesting that ASL could be an alternative for DSC-PWI. An example of ASL PWI in post-operative glioma is provided as Figure 8.

Figure 8. Post-contrast T_1 weighted images and ASL perfusion-weighted MRI overlay of glioblastoma after surgery. Panel a shows an axial post-contrast T_1 weighted image illustrating contrast-enhancement of the resection cavity borders. Panel b shows the colour-coded ASL-derived cerebral blood flow overlay image, illustrating hyperperfusion in the contrast-enhancing parts. This indicated residual tumour/tumour progression. ASL, arterial spin labelling.

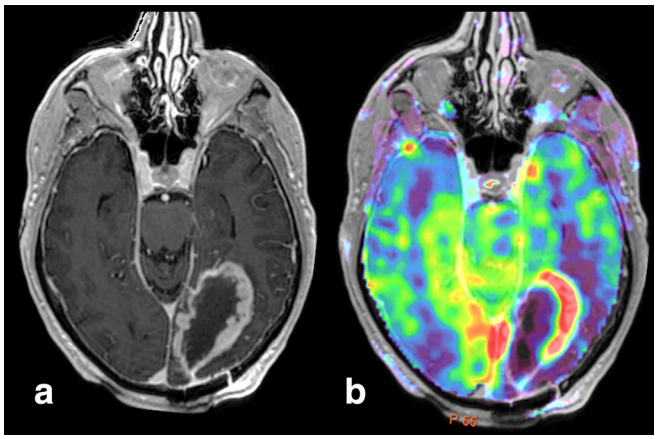

It has been reported that implementation of either DSC or DCE in routine follow-up MRI of GBM can aid the detection of tumour recurrence.[74] However, as stated above a wide range of cut-off values for each technique has been reported, which complicates further clinical implementation (*e.g.*[75–77]). Also, a variety of PWI metrics has been used in imaging trials using either PWI technique. A standardised perfusion scanning protocol and standardised methods data processing with validated criteria for the diagnostic work-up and follow-up of gliomas would contribute to more robust scientific and clinical data.[60] Efforts for standardisation of PWI acquisition have been made by various organisations (*e.g.* the American Society of Functional Neuroradiology)[78] and scientific papers.[60,79] Based on extensive simulations combined with expert knowledge, recommendations have been formulated with regard to DSC PWI (*e.g.* full-dose preload, full-dose bolus dosing using an intermediate (60°) flip-angle and choosing a field strength-dependent echo time (40–50 ms at 1.5 T, 20–35 ms at 3.0 T) in order to obtain overall best signal and precision for CBV estimates.[60] No consensus recommendations with regard to the use of DCE in neuro-oncological imaging are available. Although recommendations have been published for the use of ASL, it must be emphasised that these were not specifically designed for perfusion of neuro-oncological disease {[79] #232}. In summary, this paper recommended the use of pseudocontinuous labelling and background suppression. Also, a segmented three-dimensional readout without the use of vascular crushing gradients has been recommended {[79] #232}.

Figure 9. Single voxel MRS of glioblastoma at 1.5T. Brain MRI with axial post-contrast T_1 weighted (panel a) and T2 (panel b) images of a patient with a small T2 hyperintense space occupying cortical/subcortical lesion in the right frontal lobe with some contrast enhancement. Panel c shows the MRS spectrum of the lesion. The corresponding spectrum (acquired with TE = 20 ms) can be indicative of glioblastoma tissue. The viable tumour tissue within the region of interest is recognised by high Cho signal and decreased NAA, the spectral peaks coming from lipid signal (lactate/lipid peaks are seen around 1 ppm on the spectrum) indicate the presence of necrotic tissue, even though this is not visible on structural MRI. The most prominent signals are labelled in the spectral pattern corresponding to voxel a. Cho, Choline; Cr1/Cr2, Creatine; Ins dd1, Myo-inositol; NAA, N-acetylaspartate; TE, echo time.

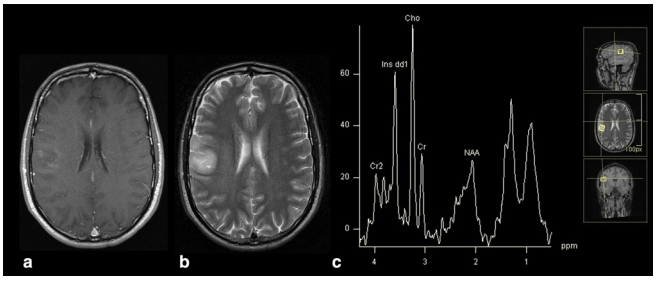

Finally, it has been shown that a well-established image-review process needs to be applied upfront to assess perfusion metrics because repeatability and reproducibility were found to be below 50 and 10% respectively in one multicentre study using DSC PWI.[80] Therefore, it has been recommended to measure rCBV in the context of clinical trials by two experienced readers. In case of disagreement, an adjudicator could be involved to provide the final perfusion measurement.[80] This is clearly time-consuming and thus impractical for clinical practice. Therefore, we recommend that PWI should be evaluated by an experienced reader and should always be interpreted together with other MRI sequences. Furthermore, radiological evolution of the area of interest over time and the clinical context of the patient should be taken into consideration when assessing PWI data.

MR SPECTROSCOPY OF GLIOBLASTOMA

The chemical composition of the tissue can be evaluated by MRS. MRS can therefore detect specific metabolites in defined regions of interest/voxels.[81,82] For GBM imaging, the most important metabolites include choline (Cho) and N-acetylaspartate (NAA) (Figure 9). In the clinical setting, MRS is often performed as a single voxel technique or as a slab comprising several voxels (*i.e.* multivoxel spectroscopy, chemical shift imaging). However, as not the entire lesion can be assessed in three dimensions at once, single voxel and multivoxel spectroscopy are known to suffer from sampling errors and outcomes can be confounded by the heterogeneous content of glioblastoma. Relatively new ^{1}H MRS sequences including 3D-echo planar spectroscopic imaging (3D EPSI) allow acquisition metabolic maps with an excellent coverage and spatial resolution. The images acquired from 3D EPSI protocols can be co-registered with anatomical images (T_1 weighted images). MRS and 3D EPSI have been described as useful imaging protocols to assess GBM metabolism and differentiation of TP from PsP.[83–87] Tumour tissue has an MRS signature of increased Cho due to the increased cell density and total cell membrane. Reduced NAA is seen due to decreased neuronal content and decreased neuronal viability. Thus, elevation of Cho and decrease of NAA is suggestive for TP, although Cho can also be elevated in patients who receive immunotherapy.[88,89] In a meta-analysis of 55 studies, MRS showed to be superior to other parametric MRI sequences (conventional, ADC, DSC PWI, DCE PWI) when differentiating PsP from TP with a pooled sensitivity/specificity of 91/95%.[73] However, this meta-analysis included a heterogeneous collection of included papers. For example, studies on MRS with single voxel and multivoxel protocols were included and compared. Furthermore, this meta-analysis made no distinction between the diagnostic capacity of the different metabolite-ratios (included were MRS studies focusing on Cho/Cre, Lac/Cho, NAA/Cho and Cho/NAA). Reported cut-off values for Cho/Cre ranged between 1.07–2.50.[90–92] The cut-off values reported for Lac/Cho and Cho/NAA were 1.05 (34) and 1.71 respectively (48). Therefore, further research is needed, preferably with well-established study reading protocols and cut-off values.

With regard to prognosis prediction, a recent MRS study showed higher Cho/NAA ratios in the post-operative peritumoral oedema zone in patients with early tumour recurrence in those areas. A higher Cho/NAA ratio in the peritumoral oedema zone was considered to be associated with poor prognosis.[93] However, this conclusion still needs to be corroborated by other research groups. 2-Hydroxyglutarate is an oncometabolite of *IDH* mutant glioma and it has recently been reported that MRS could be useful for the determination of *IDH* mutation status based on the detection of elevated levels of 2-hydroxyglutarate.[94–96] A meta-analysis on this topic found a pooled sensitivity of 84% and a pooled specificity of 97% with regard to predicting *IDH* mutation status in GBM.[97] Although promising, MRS is best carried out at 3T (or higher), requires expert knowledge and/or specific semi-automated computer-aided diagnosis software[98] and is not as widely available as other advanced MRI techniques.

^{18}F-FDG-PET IMAGING OF GLIOBLASTOMA

The use of ^{18}F-FDG-PET imaging in neuro-oncological diseases is limited by the poor tumour-to-background ratio as normal, healthy brain tissue also shows a very high physiological uptake of this tracer. Nevertheless, ^{18}F-FDG-PET can provide some useful information in GBM in research settings. For example, the maximum standardised uptake value (SUV_{max}) of ^{18}F-FDG-PET imaging could help to accurately determine the genotype of the GBM[99–102] and could help to predict patient prognosis.[100] In addition, differentiation between GBM and its main differential diagnoses (*e.g.* brain metastasis and primary central nervous system lymphoma (PCNSL)) by use of ^{18}F-FDG-PET imaging showed encouraging results.[103–106] When using cut-off values of $SUV_{max} \geq 15$, $SUV_{max} \geq 12$, and SUV_{max} of ≥9.35, a sensitivity/specificity of 88/100%, 100/71.4%, and 100/78.3%, respectively, was reported with regard to discriminating PCNSL from GBM.[107–109]

In the post-operative setting, GBM imaging by use of ^{18}F-FDG PET has been investigated by various authors to distinguish

PsP from TP.[110–118] From these studies, ^{18}F-FDG PET showed a sensitivity ranging from 68 to 100% and a specificity ranging from 33 to 100%. Reported cut-off values of SUV tumour-to-brain ratios (TBR) vary from 0.75 to 2.64 with higher values reflecting TP.[111–119] However, a more recent meta-analysis also found a statistically significantly lower pooled specificity when imaging high-grade glioma as compared to low-grade glioma (82 *vs* 90%).[119] Therefore, we conclude that FDG-PET imaging plays a limited role in post-treatment GBM imaging. Although mostly retrospective studies were carried out on this topic,[113–115] some well-performed prospective studies are also available.[117,118]

AA-PET IMAGING OF GLIOBLASTOMA

In contrast to FDG-PET imaging, radio-labelled amino-acids have a high TBR due to the increased amino-acid metabolism in GBM cells due to cell proliferation and extracellular matrix production. Therefore, AA-PET can be helpful in the imaging of GBM in the pre-operative as well as post-therapeutic setting. S-11C-methyl)-L-methionine (11C-MET), O-(2-18Ffluoroethyl)-L-tyrosine (^{18}F-FET), and 3,4-dihydroxy-6–18F-fluoro-L-phenyla lanine (^{18}F-FDOPA) are the most widely studied tracers. In the pre-operative setting, AA-PET imaging serves three main goals: primary diagnosis/differential diagnosis, glioma delineation, and treatment planning.

For ^{18}F-FET PET imaging, it has been shown that abnormal focal ^{18}F-FET uptake leads to a high sensitivity of high- grade glioma detection.[120–122] More specifically, a TBR_{max}<2.5 in ^{18}F-FET excludes a high-grade tumour with high probability.[120] It has furthermore been found that dynamic ^{18}F-FET data could be very useful for glioma grading.[123–125] Dunet et al reported that a negative slope of tumour FET time–activity was the best predictor of high-grade glioma.[125] Although several studies have been carried out with ^{11}C-MET and ^{18}F-FDOPA, these radiotracers were less accurate as compared to ^{18}F-FET.[126–128] In terms of glioma delineation, biopsy studies showed that ^{18}F-FET PET-imaging detected the extent of gliomas, including GBM, most accurately.[129,130] With regard to glioma delineation, it is known from histological validation studies that conventional MRI is limited with regard to visualising glioma extent.[129,130] TBR_{max} values of ^{18}F-FET PET imaging, on the other hand, were found to result in larger tumour volumes.[131] Similar results have been obtained with ^{18}F-FDOPA PET in progressive or recurrent GBM where a larger tumour extent was identified when compared with MRI-derived rCBV maps.[132] Accordingly, ^{18}F-FDOPA PET-based tumour volumes have been shown to extend beyond the contrast-enhancing volume on conventional MRI.[133,134]. ^{11}C-MET has only been used in the delineation of recurrent GBM indicating contrast-enhanced MRI alone resulted in an underestimation of the tumour volume.[135]

In the pre-operative setting, research showed that AA-PET imaging could be of predictive value as ^{18}F-FDOPA was found capable to predict overall survival[136] and could identify bevacizumab-responders as early as 2 weeks after treatment initiation.[137] Concerning brain biopsy planning, the use of PET imaging to identify focal hot spots has also been found relevant for GBM imaging[133,138] (Figure 10), *e.g.* for detecting

Figure 10. ^{18}F-FET PET) images of glioma in the pre-operative setting^{18}F-FET PET images show diffuse uptake of FET in the left frontoparietal lesion with focal areas of relative more uptake. These regions are thought to represent the localisations with the most high-grade tumour tissue. Biopsy was carried out and after histopathological examination, including molecular diagnostics, the diagnosis of an astrocytoma Grade III was made (according to the 2021 WHO Glioma Classification). ^{18}F-FET, O-(2-18Ffluoroethyl)-L-tyrosine; PET, positron emission tomography.

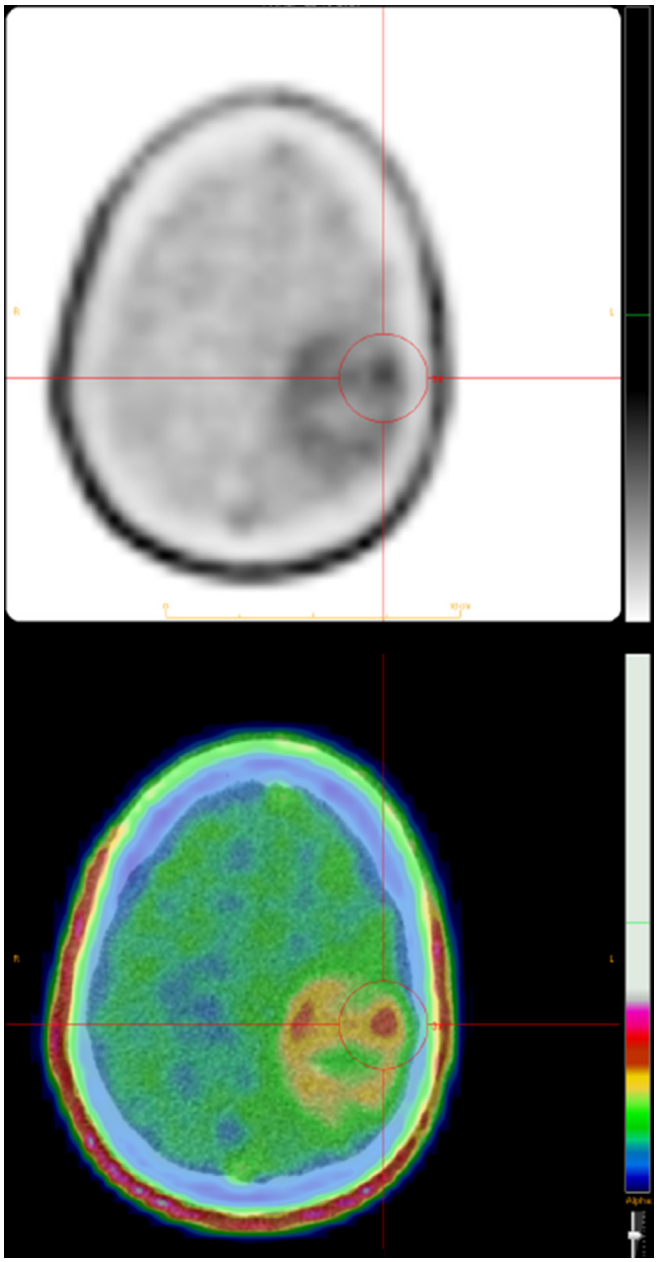

regions with abnormal activation of the *EGFR* gene due to a deletion of exons 2–7 of *EGFR*.[139] Also, AA-PET-CT was found to provide more accurate stereotactic biopsies compared to ^{18}F-FDG-PET-CT guided biopsies.[140] Studies on the use of ^{18}F-FET and ^{18}F-FDOPA to guide stereotactic biopsies showed superior results compared to ^{11}C-MET and FDG-PET guided

biopsies.[133,141,142] For instance, a recent cost-effectiveness analysis showed that the combined use of ^{18}F-FET PET and MRI resulted in a 19% higher likelihood to obtain a representative biopsy.[142] With regard to radiotherapy planning, the use of ^{11}C-MET PET imaging[143–145] and ^{18}F-FET PET imaging effectively helped to delineate areas of glioma microspread resulting in a larger target volume.[131,146,147] Nevertheless, tumour recurrence after radiotherapy was reported to occur most often within the AA-PET defined target volume.[148,149]

Additionally, the aforementioned AA-based radiotracers are widely used in the post-treatment assessment, especially with regard to differentiation of PsP from TP. Several reports presented a sensitivity/specificity ranging from 66/60 to 78/100% when distinguishing PsP from TP by use of ^{11}C-MET PET imaging.[90,119,150–159] When assessing the diagnostic accuracy of ^{18}F-FET PET imaging (see, *e.g.*[160–166]), meta-analyses reported a pooled sensitivity and specificity of 88–91% and 78–95%, respectively.[119,167] The use of ^{18}F-DOPA PET was to distinguish PsP from TP showed sensitivity and specificity ranges of 85–100% and 70–86%, respectively.[119,168–171]

With regard to research on the use of AA-PET in imaging in post-operative glioblastoma, the field is limited by the large body of retrospective studies and the unblended assessment of radiologists/nuclear medicine physicians with regard to other clinical, histopathological and imaging information.[90,113,157,158,164–166]

NOVEL MRI TECHNIQUES FOR USE IN GLIOBLASTOMA

During the last decades, tremendous developments of MRI hardware and image analysis methods allowed for micro- to macroscale imaging of GBM. These novel imaging approaches target a variety of molecular pathophysiological mechanisms occurring in GBM. To facilitate sharing of knowledge and to accelerate the clinical implementations of novel MRI techniques, the European, multidisciplinary network Glioma MR Imaging 2.0 (GliMR) was founded in 2019.[172] Although the continuous development of novel MRI techniques prevents the authors from providing a complete overview of the literature on this topic, some promising techniques are highlighted.

Diffusion kurtosis imaging (DKI) has been proposed as a sensitive method to visualise the otherwise invisible, infiltrating component of GBM. DKI is an extension of DTI methods as it provides quantitative information about how tissue water diffusion deviates from a Gaussian distributed diffusion.[173] Previous research found that DKI variables can be used to assess microstructural alterations in perilesional white matter, suggestive of tumour infiltration which is not visible on conventional MRI sequences.[174,175]

Another innovative imaging technique concerns amide proton transfer-chemical exchange saturation transfer (APT-CEST), which is aimed at assessing tumour metabolism and cell proliferation. Like other malignancies, GBM cells rewire their metabolism to grow excessively and to ensure prolonged cell-life. APT-CEST imaging indirectly visualises these mechanisms by detecting the presence of amide protons. Amide-protons accumulate in regions with an increased amount of proteins and peptides. APT-CEST imaging uses a specific radiofrequency pulse at the resonant frequency of protons inside amides (-NH). Thereby, only the protons within the amides will be saturated. In turn, the magnetic saturation of the amides will spontaneously be transferred to water due to the chemical exchange of the excited amide protons with non-excited protons within water molecules. The proton of the amides will thus be replaced with an unsaturated proton from water, causing an accumulation of saturation in water. Saturation of water will cause a decrease in water signal and is thereby an indirect reflection of amides in a target area. It has been reported that the use of APT-CEST is promising with regard to predicting *IDH* mutation status[176] and distinguishing TP from pseudoprogression.[177,178]

Deuterium metabolic imaging (DMI) is novel, non-invasive approach which combines deuterium MRS with oral intake (or intravenous injection) of non-radioactive ^{2}H-labelled substrates to generate three-dimensional metabolic maps. DMI can reveal glucose metabolism beyond uptake and thereby provides much more detailed information with regard to tissue metabolism as compared to ^{18}F-FDG-PET imaging.[179] Preliminary data showed pronounced metabolic differences between normal brain and GBM.[179]

Vessel architectural imaging (VAI) provides further insights into vessel size and type. VAI exploits the differences in observed proton relaxation from simultaneously acquired contrast-enhanced gradient recalled-echo and spin-echo MR imaging for vessel-size estimation. The temporal shift between the two relaxation curves can be used to estimate vessel type and size.[180–182] Because VAI can estimate these vessel features, it has been suggested that this technique might provide further insight into the mechanisms of pseudoprogression and the early detection of TP.[183,184]

NOVEL RADIOTRACERS FOR USE IN GLIOBLASTOMA

In recent years, several new classes of tracers have emerged that may also prove interesting for use in GBM not just from a diagnostic, but also from a therapeutic point of view as these tracers can potentially also be labelled with beta- and alpha-emitting radioisotopes. The first of these substance classes concern tracers aimed at the prostate-specific membrane antigen (PSMA). Primarily developed for use in diagnosis and therapy of metastatic prostate cancer, the inaptly named PSMA, which less colloquially is also known as glutamate carboxypeptidase two and in the brain serves as a modulator of excitatory neurotransmission, is also expressed in GBMs and their neovasculature *in vitro* as well as *in vivo*.[185–187] Although initial studies show promising results as to the diagnostic potential of PSMA in GBM,[188] no prospective data on the diagnostic value of this tracer are available as yet. However, in contrast to AA-PET, given sufficiently high uptake PSMA-PET as stated above also may indicate to possibility of radionuclide therapy with PSMA targeted substances.

The second class of interest in GBM are tracers aimed at the fibroblast activating protein (FAP). Recently introduced as a novel tracer of interest for diagnosis and possibly also therapy in a broad variety of oncological diseases,[189] this class of tracer in first, preliminary results also was shown to produce promising results in *IDH*-wildtype GBM as well as *IDH*-mutant astrocytoma, but not in low-grade *IDH*-mutant gliomas. This indicates that this class of substance may in the future play a role in non-invasively identifying high-grade *IDH*-mutant gliomas and GBMs, as well as may provide another radionuclide therapy option for these diseases.

ARTIFICIAL INTELLIGENCE AND IMAGING OF GLIOBLASTOMA

A growing number of AI-based applications is finding its way to clinical practice. Commercially available AI-based software in the field of radiology holds at least 100 CE-marked products, although the majority of these packages have not been based on peer-reviewed scientific evidence and only a minority of such software applications have demonstrated (potential) clinical impact.[190] Although AI holds the potential to perform image analyses which matches and potentially surpasses the experienced neuroradiologist's abilities,[191] important challenges for AI need to be recognised (for a review see[192]). For example, most studies on AI in GBM imaging were performed on limited sample sizes. Additionally, in most studies there was no external validation of obtained results, which limits generalisation of the study results and bears the risk of overfitting. It is therefore essential to educate the end-users on this topic, who should be familiar with the strengths and limitations for applying AI-tools in clinical practice. Also, data sharing is an important factor which will contribute to further development and implementation of AI-tools. For that reason, the open-access imaging databases of the MICCAI[193] and the Erasmus Glioma Database[194] are much needed advances in this field. Creating and maintaining such large databases are essential, though time-intensive tasks. AI could also play a role in data curation in order to preserve its integrity and ensure reusability.[195]

The potential of AI tools in glioma image analysis is also immense. First, AI-based glioma segmentation was found to be highly accurate,[196] which would relieve radiologists of the labour-intensive task of image segmentation or even tumour measurement. This explains why fully automated segmentation tools have gained interest over the years and highlights the importance of the annual multimodal Brain Tumour Segmentation (BraTS) challenge (http://braintumorsegmentation.org/). A recent report showed that the implementation of an AI- based segmentation tool in our clinical practice resulted in reasonable (77%) rates of successful segmentation.[197]

In one study, researchers used an AI application as an add-on feature in radiological readings to predict *IDH* mutation status in gliomas.[198] In this study, neuroradiologists' predictive capacity of WHO grade was improved when coupled with the predictive capacities of a random forest algorithm. In addition, the same input variables could be used to accurately predicting *IDH* mutation status.[198] Two recent meta-analysis on this subject provided an overview of the accuracy of AI with regard to predicting glioma genomics, which showed high accuracy of machine learning algorithms for the prediction of *IDH* mutation status, 1p/19q codeletion status, *MGMT* promoter mutation and *TERT* promoter mutation with AUROCs of 0.909, 0.748, 0.866 and 0.842, respectively.[199] However, again these studies mainly used internal validation and external validation was largely lacking. In a recent review, similar predictive capacities were found with pooled sensitivities and specificities of 0.88, 0.76 and 0.76 for predicting *IDH* mutation status, 1p/19q codeletion status and *MGMT* promoter mutation, respectively.[200] Pooled specificity for predicting *IDH* mutation status, 1p/19q codeletion status and *MGMT* promoter mutation showed to 0.86, 0.83 and 0.83, respectively. However, these meta-data represent the predictive capacities of the investigated artificial intelligence approaches in their training phase. With regard to the *IDH* mutation status, a meta-analysis was provided on the diagnostic accuracy parameters in the (mostly internal) validation sets. The pooled sensitivity and specificity for predicting *IDH* mutation status were 0.83 and 0.85 in validation sets, respectively.[200]

RECOMMENDATIONS AND CONCLUSIONS

From the published literature, it is evident that advanced neuroimaging techniques have the potential to add value to the diagnostic work-up, treatment planning and surveillance of patients with suspected GBM. It is, however, also clear that there is wide variability in their application and interpretation, while patient access to these techniques also varies widely.[201] With the exception of the newly defined response assessment criteria for paediatric low-grade glioma—which include DWI—advanced imaging techniques are not part of international and widely accepted response assessment criteria such as those defined by the Response Assessment for Neuro Oncology (RANO) working groups. This can at least in part be attributed to the lack of standardisation and high-level evidence. Most published work concerns retrospective, selected and often small patient populations, while prospective studies—in particular using external validation cohorts—are rare and randomised controlled trials non-existent. Here, we find ourselves somewhat in a Catch-22: due to the fact that advanced imaging is not part of response assessment criteria, there is no harmonised guidance on its use, while at the same time, the lack of standardisation severely hampers the definition of uniform guidelines. Recent international efforts to standardise image acquisition in glioma[5,202] are instrumental to break this vicious circle and to facilitate studies for obtaining the much needed high-level evidence for providing clear guidance on the optimal choice and application of the various advanced imaging techniques.

At the same time, it seems that PWI and MRS, as well as AA-PET have found widespread application for diagnostic challenges, in particular for assessing tumour aggressiveness, extent, and differentiation from treatment-related effects, while DWI has its particular use for differential diagnosis and pre-surgical tractography. Novel tracers aimed at PSMA or FAP could mix up the landscape here as these tracers also seem to have specific diagnostic properties as well as the potential for radionuclide therapy. It remains to be seen if and which technique is superior to others,

and until such time individual institutions apply techniques according to local preferences and expertise. In the absence of a clearly superior technique, the local level of expertise is probably a more important factor than the choice of technique. This also means that the acquisition, post-processing, and interpretation need to be in the hands of experts who are not only technically but also clinically informed on the strengths *and* weaknesses of each applied technique.

The same could be said about AI-based tools, which have enormous potential to improve and enhance clinical practice, on the one hand automating tasks that are currently done manually (such as tumour segmentation) and on the other hand providing additional diagnostic information (such as prediction of tumour genotype). Again, levels of evidence are still low and the time is now ripe for studies with prospective, sufficiently powered cohorts and—crucially—external validation. Guidance for setting up and assessing the strength of AI studies is for instance provided by the radiomics quality score.[203]

The classification of diffuse glioma, including GBM, is a rapidly changing the landscape with an important role for diagnostic imaging at every step along the way from diagnosis to treatment decision-making and treatment monitoring. Advanced imaging acquisition and AI-based analyses provide powerful tools, both in their current form and in future developments, but need to be used with expert knowledge within the context of the currently available evidence.

REFERENCES

1. Dolecek TA, Propp JM, Stroup NE, Kruchko C. CBTRUS statistical report: primary brain and central nervous system tumors diagnosed in the united states in 2005-2009. *Neuro Oncol* 2012; **14 Suppl 5**: v1–49. https://doi.org/10.1093/neuonc/nos218
2. Lapointe S, Perry A, Butowski NA. Primary brain tumours in adults. *Lancet* 2018; **392**: 432–46. https://doi.org/10.1016/S0140-6736(18)30990-5
3. Louis DN, Perry A, Wesseling P, Brat DJ, Cree IA, Figarella-Branger D, et al. The 2021 WHO classification of tumors of the central nervous system: a summary. *Neuro Oncol* 2021; **23**: 1231–51. https://doi.org/10.1093/neuonc/noab106
4. Louis DN, Perry A, Reifenberger G, von Deimling A, Figarella-Branger D, Cavenee WK, et al. The 2016 world health organization classification of tumors of the central nervous system: a summary. *Acta Neuropathol* 2016; **131**: 803–20. https://doi.org/10.1007/s00401-016-1545-1
5. Ellingson BM, Bendszus M, Boxerman J, Barboriak D, Erickson BJ, Smits M, et al. Consensus recommendations for a standardized brain tumor imaging protocol in clinical trials. *Neuro Oncol* 2015; **17**: 1188–98. https://doi.org/10.1093/neuonc/nov095
6. Chang P, Grinband J, Weinberg BD, Bardis M, Khy M, Cadena G, et al. Deep-learning convolutional neural networks accurately classify genetic mutations in gliomas. *AJNR Am J Neuroradiol* 2018; **39**: 1201–7. https://doi.org/10.3174/ajnr.A5667
7. Carrillo JA, Lai A, Nghiemphu PL, Kim HJ, Phillips HS, Kharbanda S, et al. Relationship between tumor enhancement, edema, IDH1 mutational status, MGMT promoter methylation, and survival in glioblastoma. *AJNR Am J Neuroradiol* 2012; **33**: 1349–55. https://doi.org/10.3174/ajnr.A2950
8. Hong EK, Choi SH, Shin DJ, Jo SW, Yoo R-E, Kang KM, et al. Radiogenomics correlation between MR imaging features and major genetic profiles in glioblastoma. *Eur Radiol* 2018; **28**: 4350–61. https://doi.org/10.1007/s00330-018-5400-8
9. Altieri R, Zenga F, Ducati A, Melcarne A, Cofano F, Mammi M, et al. Tumor location and patient age predict biological signatures of high-grade gliomas. *Neurosurg Rev* 2018; **41**: 599–604. https://doi.org/10.1007/s10143-017-0899-8
10. Tejada Neyra MA, Neuberger U, Reinhardt A, Brugnara G, Bonekamp D, Sill M, et al. Voxel-wise radiogenomic mapping of tumor location with key molecular alterations in patients with glioma. *Neuro Oncol* 2018; **20**: 1517–24. https://doi.org/10.1093/neuonc/noy134
11. Thon N, Kreth S, Kreth FW. Personalized treatment strategies in glioblastoma: MGMT promoter methylation status. *Onco Targets Ther* 2013; **6**: 1363–72. https://doi.org/10.2147/OTT.S50208
12. Mulholland S, Pearson DM, Hamoudi RA, Malley DS, Smith CM, Weaver JMJ, et al. MGMT cpg island is invariably methylated in adult astrocytic and oligodendroglial tumors with IDH1 or IDH2 mutations. *Int J Cancer* 2012; **131**: 1104–13. https://doi.org/10.1002/ijc.26499
13. Yoon RG, Kim HS, Paik W, Shim WH, Kim SJ, Kim JH. Different diagnostic values of imaging parameters to predict pseudoprogression in glioblastoma subgroups stratified by MGMT promoter methylation. *Eur Radiol* 2017; **27**: 255–66. https://doi.org/10.1007/s00330-016-4346-y
14. Ellingson BM, Lai A, Harris RJ, Selfridge JM, Yong WH, Das K, et al. Probabilistic radiographic atlas of glioblastoma phenotypes. *AJNR Am J Neuroradiol* 2013; **34**: 533–40. https://doi.org/10.3174/ajnr.A3253
15. Patel SH, Poisson LM, Brat DJ, Zhou Y, Cooper L, Snuderl M, et al. T2-FLAIR mismatch, an imaging biomarker for IDH and 1p/19q status in lower-grade gliomas: A TCGA/TCIA project. *Clin Cancer Res* 2017; **23**: 6078–85. https://doi.org/10.1158/1078-0432.CCR-17-0560
16. Broen MPG, Smits M, Wijnenga MMJ, Dubbink HJ, Anten MHME, Schijns OEMG, et al. The T2-FLAIR mismatch sign as an imaging marker for non-enhancing IDH-mutant, 1p/19q-intact lower-grade glioma: a validation study. *Neuro Oncol* 2018; **20**: 1393–99. https://doi.org/10.1093/neuonc/noy048
17. Smits M. Imaging of oligodendroglioma. *Br J Radiol* 2016; **89**: 20150857: 1060: . https://doi.org/10.1259/bjr.20150857
18. van den Bent MJ, Smits M, Kros JM, Chang SM. Diffuse infiltrating oligodendroglioma and astrocytoma. *J Clin Oncol* 2017; **35**: 2394–2401. https://doi.org/10.1200/JCO.2017.72.6737
19. Jenkinson MD, du Plessis DG, Smith TS, Joyce KA, Warnke PC, Walker C. Histological growth patterns and genotype in oligodendroglial tumours: correlation with MRI features. *Brain* 2006; **129**: 1884–91. https://doi.org/10.1093/brain/awl108
20. Zikou A, Sioka C, Alexiou GA, Fotopoulos A, Voulgaris S, Argyropoulou MI. Radiation necrosis, pseudoprogression, pseudoresponse, and tumor recurrence: imaging challenges for the evaluation of treated gliomas. *Contrast Media Mol*

Imaging 2018; **2018**: 6828396. https://doi.org/10.1155/2018/6828396
21. Young RJ, Gupta A, Shah AD, Graber JJ, Zhang Z, Shi W, et al. Potential utility of conventional MRI signs in diagnosing pseudoprogression in glioblastoma. *Neurology* 2011; **76**: 1918–24. https://doi.org/10.1212/WNL.0b013e31821d74e7
22. Bammer R. Basic principles of diffusion-weighted imaging. *Eur J Radiol* 2003; **45**: 169–84. https://doi.org/10.1016/s0720-048x(02)00303-0
23. Sugahara T, Korogi Y, Kochi M, Ikushima I, Shigematu Y, Hirai T, et al. Usefulness of diffusion-weighted MRI with echo-planar technique in the evaluation of cellularity in gliomas. *J Magn Reson Imaging* 1999; **9**: 53–60. https://doi.org/10.1002/(sici)1522-2586(199901)9:1<53::aid-jmri7>3.0.co;2-2
24. Ellingson BM, Malkin MG, Rand SD, Connelly JM, Quinsey C, LaViolette PS, et al. Validation of functional diffusion maps (fdms) as a biomarker for human glioma cellularity. *J Magn Reson Imaging* 2010; **31**: 538–48. https://doi.org/10.1002/jmri.22068
25. Farace P, Amelio D, Ricciardi GK, Zoccatelli G, Magon S, Pizzini F, et al. Early MRI changes in glioblastoma in the period between surgery and adjuvant therapy. *J Neurooncol* 2013; **111**: 177–85. https://doi.org/10.1007/s11060-012-0997-y
26. Chang PD, Chow DS, Yang PH, Filippi CG, Lignelli A. Predicting glioblastoma recurrence by early changes in the apparent diffusion coefficient value and signal intensity on FLAIR images. *AJR Am J Roentgenol* 2017; **208**: 57–65. https://doi.org/10.2214/AJR.16.16234
27. Buemi F, Guzzardi G, Del Sette B, Sponghini AP, Matheoud R, Soligo E, et al. Apparent diffusion coefficient and tumor volume measurements help stratify progression-free survival of bevacizumab-treated patients with recurrent glioblastoma multiforme. *Neuroradiol J* 2019; **32**: 241–49. https://doi.org/10.1177/1971400919847184
28. Patel KS, Everson RG, Yao J, Raymond C, Goldman J, Schlossman J, et al. Diffusion magnetic resonance imaging phenotypes predict overall survival benefit from bevacizumab or surgery in recurrent glioblastoma with large tumor burden. *Neurosurgery* 2020; **87**: 931–38. https://doi.org/10.1093/neuros/nyaa135
29. Park JE, Kim HS, Park SY, Jung SC, Kim JH, Heo HY. Identification of early response to anti-angiogenic therapy in recurrent glioblastoma: amide proton transfer-weighted and perfusion-weighted MRI compared with diffusion-weighted MRI. *Radiology* 2020; **295**: 397–406. https://doi.org/10.1148/radiol.2020191376
30. Kim BS, Kim ST, Kim JH, Seol HJ, Nam D-H, Shin HJ, et al. Apparent diffusion coefficient as a predictive biomarker for survival in patients with treatment-naive glioblastoma using quantitative multiparametric magnetic resonance profiling. *World Neurosurg* 2019; **122**: e812–20. https://doi.org/10.1016/j.wneu.2018.10.151
31. Romano A, Calabria LF, Tavanti F, Minniti G, Rossi-Espagnet MC, Coppola V, et al. Apparent diffusion coefficient obtained by magnetic resonance imaging as a prognostic marker in glioblastomas: correlation with MGMT promoter methylation status. *Eur Radiol* 2013; **23**: 513–20. https://doi.org/10.1007/s00330-012-2601-4
32. Auer TA, Breit H-C, Marini F, Renovanz M, Ringel F, Sommer CJ, et al. Evaluation of the apparent diffusion coefficient in patients with recurrent glioblastoma under treatment with bevacizumab with radiographic pseudoresponse. *J Neuroradiol* 2019; **46**: 36–43. https://doi.org/10.1016/j.neurad.2018.04.002
33. Zeng QS, Li CF, Liu H, Zhen JH, Feng DC. Distinction between recurrent glioma and radiation injury using magnetic resonance spectroscopy in combination with diffusion-weighted imaging. *Int J Radiat Oncol Biol Phys* 2007; **68**: 151–58. https://doi.org/10.1016/j.ijrobp.2006.12.001
34. Xu J-L, Li Y-L, Lian J-M, Dou S, Yan F-S, Wu H, et al. Distinction between postoperative recurrent glioma and radiation injury using MR diffusion tensor imaging. *Neuroradiology* 2010; **52**: 1193–99. https://doi.org/10.1007/s00234-010-0731-4
35. Lee WJ, Choi SH, Park C-K, Yi KS, Kim TM, Lee S-H, et al. Diffusion-weighted MR imaging for the differentiation of true progression from pseudoprogression following concomitant radiotherapy with temozolomide in patients with newly diagnosed high-grade gliomas. *Acad Radiol* 2012; **19**: 1353–61. https://doi.org/10.1016/j.acra.2012.06.011
36. Song YS, Choi SH, Park C-K, Yi KS, Lee WJ, Yun TJ, et al. True progression versus pseudoprogression in the treatment of glioblastomas: A comparison study of normalized cerebral blood volume and apparent diffusion coefficient by histogram analysis. *Korean J Radiol* 2013; **14**: 662–72. https://doi.org/10.3348/kjr.2013.14.4.662
37. Chu HH, Choi SH, Ryoo I, Kim SC, Yeom JA, Shin H, et al. Differentiation of true progression from pseudoprogression in glioblastoma treated with radiation therapy and concomitant temozolomide: comparison study of standard and high-b-value diffusion-weighted imaging. *Radiology* 2013; **269**: 831–40. https://doi.org/10.1148/radiol.13122024
38. Prager AJ, Martinez N, Beal K, Omuro A, Zhang Z, Young RJ. Diffusion and perfusion MRI to differentiate treatment-related changes including pseudoprogression from recurrent tumors in high-grade gliomas with histopathologic evidence. *AJNR Am J Neuroradiol* 2015; **36**: 877–85. https://doi.org/10.3174/ajnr.A4218
39. Kazda T, Bulik M, Pospisil P, Lakomy R, Smrcka M, Slampa P, et al. Advanced MRI increases the diagnostic accuracy of recurrent glioblastoma: single institution thresholds and validation of MR spectroscopy and diffusion weighted MR imaging. *Neuroimage Clin* 2016; **11**: 316–21. https://doi.org/10.1016/j.nicl.2016.02.016
40. Zakhari N, Taccone MS, Torres C, Chakraborty S, Sinclair J, Woulfe J, et al. Diagnostic accuracy of centrally restricted diffusion in the differentiation of treatment-related necrosis from tumor recurrence in high-grade gliomas. *AJNR Am J Neuroradiol* 2018; **39**: 260–64. https://doi.org/10.3174/ajnr.A5485
41. Yang Y, Yang Y, Wu X, Pan Y, Zhou D, Zhang H, et al. Adding DSC PWI and DWI to BT-RADS can help identify postoperative recurrence in patients with high-grade gliomas. *J Neurooncol* 2020; **146**: 363–71. https://doi.org/10.1007/s11060-019-03387-6
42. Park YW, Ahn SS, Kim EH, Kang S-G, Chang JH, Kim SH, et al. Differentiation of recurrent diffuse glioma from treatment-induced change using amide proton transfer imaging: incremental value to diffusion and perfusion parameters. *Neuroradiology* 2021; **63**: 363–72. https://doi.org/10.1007/s00234-020-02542-5
43. Lee WJ, Choi SH, Park C-K, Yi KS, Kim TM, Lee S-H, et al. Diffusion-weighted MR imaging for the differentiation of true progression from pseudoprogression following concomitant radiotherapy with temozolomide in patients with newly diagnosed high-grade gliomas. *Acad Radiol* 2012; **19**: 1353–61. https://doi.org/10.1016/j.acra.2012.06.011
44. Kazda T, Bulik M, Pospisil P, Lakomy R, Smrcka M, Slampa P, et al. Advanced MRI increases the diagnostic accuracy of recurrent glioblastoma: single institution thresholds and validation of MR spectroscopy and diffusion weighted MR imaging. *Neuroimage Clin* 2016; **11**: 316–21. https://doi.org/10.1016/j.nicl.2016.02.016

45. Yang Y, Yang Y, Wu X, Pan Y, Zhou D, Zhang H, et al. Adding DSC PWI and DWI to BT-RADS can help identify postoperative recurrence in patients with high-grade gliomas. *J Neurooncol* 2020; **146**: 363–71. https://doi.org/10.1007/s11060-019-03387-6
46. Park YW, Ahn SS, Kim EH, Kang S-G, Chang JH, Kim SH, et al. Differentiation of recurrent diffuse glioma from treatment-induced change using amide proton transfer imaging: incremental value to diffusion and perfusion parameters. *Neuroradiology* 2021; **63**: 363–72. https://doi.org/10.1007/s00234-020-02542-5
47. O'Donnell LJ, Westin C-F. An introduction to diffusion tensor image analysis. *Neurosurg Clin N Am* 2011; **22**: 185–96. https://doi.org/10.1016/j.nec.2010.12.004
48. Jellison BJ, Field AS, Medow J, Lazar M, Salamat MS, Alexander AL. Diffusion tensor imaging of cerebral white matter: a pictorial review of physics, fiber tract anatomy, and tumor imaging patterns. *AJNR Am J Neuroradiol* 2004; **25**: 356–69.
49. Henderson F, Abdullah KG, Verma R, Brem S. Tractography and the connectome in neurosurgical treatment of gliomas: the premise, the progress, and the potential. *Neurosurg Focus* 2020; **48**: 2019.11.FOCUS19785. https://doi.org/10.3171/2019.11.FOCUS19785
50. Mohan S, Wang S, Coban G, Kural F, Chawla S, O'Rourke DM, et al. Detection of occult neoplastic infiltration in the corpus callosum and prediction of overall survival in patients with glioblastoma using diffusion tensor imaging. *Eur J Radiol* 2019; **112**: 106–11. https://doi.org/10.1016/j.ejrad.2019.01.015
51. Peeken JC, Molina-Romero M, Diehl C, Menze BH, Straube C, Meyer B, et al. Deep learning derived tumor infiltration maps for personalized target definition in glioblastoma radiotherapy. *Radiother Oncol* 2019; **138**: 166–72. https://doi.org/10.1016/j.radonc.2019.06.031
52. Esmaeili M, Stensjøen AL, Berntsen EM, Solheim O, Reinertsen I. The direction of tumour growth in glioblastoma patients. *Sci Rep* 2018; **8**(1): 1199. https://doi.org/10.1038/s41598-018-19420-z
53. Wang S, Martinez-Lage M, Sakai Y, Chawla S, Kim SG, Alonso-Basanta M, et al. Differentiating tumor progression from pseudoprogression in patients with glioblastomas using diffusion tensor imaging and dynamic susceptibility contrast MRI. *AJNR Am J Neuroradiol* 2016; **37**: 28–36. https://doi.org/10.3174/ajnr.A4474
54. Razek A, El-Serougy L, Abdelsalam M, Gaballa G, Talaat M. Differentiation of residual/recurrent gliomas from postradiation necrosis with arterial spin labeling and diffusion tensor magnetic resonance imaging-derived metrics. *Neuroradiology* 2018; **60**: 169–77. https://doi.org/10.1007/s00234-017-1955-3
55. Xu J-L, Li Y-L, Lian J-M, Dou S, Yan F-S, Wu H, et al. Distinction between postoperative recurrent glioma and radiation injury using MR diffusion tensor imaging. *Neuroradiology* 2010; **52**: 1193–99. https://doi.org/10.1007/s00234-010-0731-4
56. Wang S, Martinez-Lage M, Sakai Y, Chawla S, Kim SG, Alonso-Basanta M, et al. Differentiating tumor progression from pseudoprogression in patients with glioblastomas using diffusion tensor imaging and dynamic susceptibility contrast MRI. *AJNR Am J Neuroradiol* 2016; **37**: 28–36. https://doi.org/10.3174/ajnr.A4474
57. Wang N, Jain RK, Batchelor TT. New directions in anti-angiogenic therapy for glioblastoma. *Neurotherapeutics* 2017; **14**: 321–32. https://doi.org/10.1007/s13311-016-0510-y
58. Essig M, Shiroishi MS, Nguyen TB, Saake M, Provenzale JM, Enterline D, et al. Perfusion MRI: the five most frequently asked technical questions. *AJR Am J Roentgenol* 2013; **200**: 24–34. https://doi.org/10.2214/AJR.12.9543
59. Petrella JR, Provenzale JM. MR perfusion imaging of the brain: techniques and applications. *AJR Am J Roentgenol* 2000; **175**: 207–19. https://doi.org/10.2214/ajr.175.1.1750207
60. Boxerman JL, Quarles CC, Hu LS, Erickson BJ, Gerstner ER, Smits M, et al. Consensus recommendations for a dynamic susceptibility contrast MRI protocol for use in high-grade gliomas. *Neuro Oncol* 2020; **22**: 1262–75. https://doi.org/10.1093/neuonc/noaa141
61. Oei MTH, Meijer FJA, Mordang J-J, Smit EJ, Idema AJS, Goraj BM, et al. Observer variability of reference tissue selection for relativecerebral blood volume measurements in glioma patients. *Eur Radiol* 2018; **28**: 3902–11. https://doi.org/10.1007/s00330-018-5353-y
62. Cha S, Knopp EA, Johnson G, Wetzel SG, Litt AW, Zagzag D. Intracranial mass lesions: dynamic contrast-enhanced susceptibility-weighted echo-planar perfusion MR imaging. *Radiology* 2002; **223**: 11–29. https://doi.org/10.1148/radiol.2231010594
63. Amukotuwa SA, Yu C, Zaharchuk G. 3D pseudocontinuous arterial spin labeling in routine clinical practice: A review of clinically significant artifacts. *J Magn Reson Imaging* 2016; **43**: 11–27. https://doi.org/10.1002/jmri.24873
64. Grade M, Hernandez Tamames JA, Pizzini FB, Achten E, Golay X, Smits M. A neuroradiologist's guide to arterial spin labeling MRI in clinical practice. *Neuroradiology* 2015; **57**: 1181–1202. https://doi.org/10.1007/s00234-015-1571-z
65. Haller S, Zaharchuk G, Thomas DL, Lovblad KO, Barkhof F, Golay X. Arterial spin labeling perfusion of the brain: emerging clinical applications. *Radiology* 2016; **281**: 337–56. https://doi.org/10.1148/radiol.2016150789
66. van Santwijk L, Kouwenberg V, Meijer F, Smits M, Henssen D. A systematic review and meta-analysis on the differentiation of glioma grade and mutational status by use of perfusion-based magnetic resonance imaging. *Insights Imaging* 2022; **13**(1): 102. https://doi.org/10.1186/s13244-022-01230-7
67. Alsaedi A, Doniselli F, Jäger HR, Panovska-Griffiths J, Rojas-Garcia A, Golay X, et al. The value of arterial spin labelling in adults glioma grading: systematic review and meta-analysis. *Oncotarget* 2019; **10**: 1589–1601. https://doi.org/10.18632/oncotarget.26674
68. Çoban G, Mohan S, Kural F, Wang S, O'Rourke DM, Poptani H. Prognostic value of dynamic susceptibility contrast-enhanced and diffusion-weighted MR imaging in patients with glioblastomas. *AJNR Am J Neuroradiol* 2015; **36**: 1247–52. https://doi.org/10.3174/ajnr.A4284
69. Rau MK, Braun C, Skardelly M, Schittenhelm J, Paulsen F, Bender B, et al. Prognostic value of blood flow estimated by arterial spin labeling and dynamic susceptibility contrast-enhanced MR imaging in high-grade gliomas. *J Neurooncol* 2014; **120**: 557–66. https://doi.org/10.1007/s11060-014-1586-z
70. Kim SH, Cho KH, Choi SH, Kim TM, Park CK, Park SH, et al. Prognostic predictions for patients with glioblastoma after standard treatment: application of contrast leakage information from DSC-MRI within nonenhancing FLAIR high-signal-intensity lesions. *AJNR Am J Neuroradiol* 2019; **40**: 2052–58. https://doi.org/10.3174/ajnr.A6297
71. Romano A, Pasquini L, Di Napoli A, Tavanti F, Boellis A, Rossi Espagnet MC, et al. Prediction of survival in patients affected by glioblastoma: histogram analysis of perfusion MRI. *J Neurooncol* 2018; **139**: 455–60. https://doi.org/10.1007/s11060-018-2887-4
72. Patel P, Baradaran H, Delgado D, Askin G, Christos P, John Tsiouris A, et al. MR perfusion-weighted imaging in the

evaluation of high-grade gliomas after treatment: a systematic review and meta-analysis. *Neuro Oncol* 2017; **19**: 118–27. https://doi.org/10.1093/neuonc/now148
73. van Dijken BRJ, van Laar PJ, Holtman GA, van der Hoorn A. Diagnostic accuracy of magnetic resonance imaging techniques for treatment response evaluation in patients with high-grade glioma, a systematic review and meta-analysis. *Eur Radiol* 2017; **27**: 4129–44. https://doi.org/10.1007/s00330-017-4789-9
74. Kim HS, Goh MJ, Kim N, Choi CG, Kim SJ, Kim JH. Which combination of MR imaging modalities is best for predicting recurrent glioblastoma? study of diagnostic accuracy and reproducibility. *Radiology* 2014; **273**: 831–43. https://doi.org/10.1148/radiol.14132868
75. Young RJ, Gupta A, Shah AD, Graber JJ, Chan TA, Zhang Z, et al. MRI perfusion in determining pseudoprogression in patients with glioblastoma. *Clin Imaging* 2013; **37**: 41–49. https://doi.org/10.1016/j.clinimag.2012.02.016
76. Nael K, Bauer AH, Hormigo A, Lemole M, Germano IM, Puig J, et al. Multiparametric MRI for differentiation of radiation necrosis from recurrent tumor in patients with treated glioblastoma. *AJR Am J Roentgenol* 2018; **210**: 18–23. https://doi.org/10.2214/AJR.17.18003
77. Di Costanzo A, Scarabino T, Trojsi F, Popolizio T, Bonavita S, de Cristofaro M, et al. Recurrent glioblastoma multiforme versus radiation injury: a multiparametric 3-T MR approach. *Radiol Med* 2014; **119**: 616–24. https://doi.org/10.1007/s11547-013-0371-y
78. Welker K, Boxerman J, Kalnin A, Kaufmann T, Shiroishi M, Wintermark M, et al. ASFNR recommendations for clinical performance of MR dynamic susceptibility contrast perfusion imaging of the brain. *AJNR Am J Neuroradiol* 2015; **36**: E41–51. https://doi.org/10.3174/ajnr.A4341
79. Alsop DC, Detre JA, Golay X, Gunther M, Hendrikse J, Hernandez-Garcia L, et al. Recommended implementation of arterial spin-labeled perfusion MRI for clinical applications: A consensus of the ISMRM perfusion study group and the european consortium for ASL in dementia. *Magn Reson Med* 2015; **73**: 102–16. https://doi.org/10.1002/mrm.25197
80. Smits M, Bendszus M, Collette S, Postma LA, Dhermain F, Hagenbeek RE, et al. Repeatability and reproducibility of relative cerebral blood volume measurement of recurrent glioma in a multicentre trial setting. *Eur J Cancer* 2019; **114**: 89–96. https://doi.org/10.1016/j.ejca.2019.03.007
81. Castillo M, Kwock L, Mukherji SK. Clinical applications of proton MR spectroscopy. *AJNR Am J Neuroradiol* 1996; **17**: 1–15.
82. van der Graaf M. In vivo magnetic resonance spectroscopy: basic methodology and clinical applications. *Eur Biophys J* 2010; **39**: 527–40. https://doi.org/10.1007/s00249-009-0517-y
83. Chawla S, Oleaga L, Wang S, Krejza J, Wolf RL, Woo JH, et al. Role of proton magnetic resonance spectroscopy in differentiating oligodendrogliomas from astrocytomas. *J Neuroimaging* 2010; **20**: 3–8. https://doi.org/10.1111/j.1552-6569.2008.00307.x
84. Chawla S, Wang S, Wolf RL, Woo JH, Wang J, O'Rourke DM, et al. Arterial spin-labeling and MR spectroscopy in the differentiation of gliomas. *AJNR Am J Neuroradiol* 2007; **28**: 1683–89. https://doi.org/10.3174/ajnr.A0673
85. Bulik M, Jancalek R, Vanicek J, Skoch A, Mechl M. Potential of MR spectroscopy for assessment of glioma grading. *Clin Neurol Neurosurg* 2013; **115**: 146–53. https://doi.org/10.1016/j.clineuro.2012.11.002
86. Mohan S, Chawla S, Wang S, Verma G, Skolnik A, Brem S, et al. Assessment of early response to tumor-treating fields in newly diagnosed glioblastoma using physiologic and metabolic MRI: initial experience. *CNS Oncol* 2016; **5**: 137–44. https://doi.org/10.2217/cns-2016-0003
87. Verma G, Chawla S, Mohan S, Wang S, Nasrallah M, Sheriff S, et al. Three-dimensional echo planar spectroscopic imaging for differentiation of true progression from pseudoprogression in patients with glioblastoma. *NMR Biomed* 2019; **32**(2): e4042. https://doi.org/10.1002/nbm.4042
88. Mader I, Rauer S, Gall P, Klose U. (1)H MR spectroscopy of inflammation, infection and ischemia of the brain. *Eur J Radiol* 2008; **67**: 250–57. https://doi.org/10.1016/j.ejrad.2008.02.033
89. Aquino D, Gioppo A, Finocchiaro G, Bruzzone MG, Cuccarini V. MRI in glioma immunotherapy: evidence, pitfalls, and perspectives. *J Immunol Res* 2017; **2017**: 5813951. https://doi.org/10.1155/2017/5813951
90. D'Souza MM, Sharma R, Jaimini A, Panwar P, Saw S, Kaur P, et al. 11C-MET PET/CT and advanced MRI in the evaluation of tumor recurrence in high-grade gliomas. *Clin Nucl Med* 2014; **39**: 791–98. https://doi.org/10.1097/RLU.0000000000000532
91. Seeger A, Braun C, Skardelly M, Paulsen F, Schittenhelm J, Ernemann U, et al. Comparison of three different MR perfusion techniques and MR spectroscopy for multiparametric assessment in distinguishing recurrent high-grade gliomas from stable disease. *Acad Radiol* 2013; **20**: 1557–65. https://doi.org/10.1016/j.acra.2013.09.003
92. Zeng QS, Li CF, Zhang K, Liu H, Kang XS, Zhen JH. Multivoxel 3D proton MR spectroscopy in the distinction of recurrent glioma from radiation injury. *J Neurooncol* 2007; **84**: 63–69. https://doi.org/10.1007/s11060-007-9341-3
93. Cui Y, Zeng W, Jiang H, Ren X, Lin S, Fan Y, et al. Higher cho/NAA ratio in postoperative peritumoral edema zone is associated with earlier recurrence of glioblastoma. *Front Neurol* 2020; **11**: 592155. https://doi.org/10.3389/fneur.2020.592155
94. Di Ieva A, Magnussen JS, McIntosh J, Mulcahy MJ, Pardey M, Choi C. Magnetic resonance spectroscopic assessment of isocitrate dehydrogenase status in gliomas: the new frontiers of spectrobiopsy in neurodiagnostics. *World Neurosurg* 2020; **133**: e421–27. https://doi.org/10.1016/j.wneu.2019.09.040
95. Pope WB, Prins RM, Albert Thomas M, Nagarajan R, Yen KE, Bittinger MA, et al. Non-invasive detection of 2-hydroxyglutarate and other metabolites in IDH1 mutant glioma patients using magnetic resonance spectroscopy. *J Neurooncol* 2012; **107**: 197–205. https://doi.org/10.1007/s11060-011-0737-8
96. Choi C, Raisanen JM, Ganji SK, Zhang S, McNeil SS, An Z, et al. Prospective longitudinal analysis of 2-hydroxyglutarate magnetic resonance spectroscopy identifies broad clinical utility for the management of patients with IDH-mutant glioma. *J Clin Oncol* 2016; **34**: 4030–39. https://doi.org/10.1200/JCO.2016.67.1222
97. Bhandari A, Sharma C, Ibrahim M, Riggs M, Jones R, Lasocki A. The role of 2-hydroxyglutarate magnetic resonance spectroscopy for the determination of isocitrate dehydrogenase status in lower grade gliomas versus glioblastoma: a systematic review and meta-analysis of diagnostic test accuracy. *Neuroradiology* 2021; **63**: 1823–30. https://doi.org/10.1007/s00234-021-02702-1
98. [cited 2021 2nd November]; Available from. Available from: http://s-provencher.com/lcmodel.shtml
99. Albert NL, Weller M, Suchorska B, Galldiks N, Soffietti R, Kim MM, et al. Response assessment in neuro-oncology working group and european association for neuro-oncology recommendations for the clinical

use of PET imaging in gliomas. *Neuro Oncol* 2016; **18**: 1199–1208. https://doi.org/10.1093/neuonc/now058

100. Herholz K. Brain tumors: an update on clinical PET research in gliomas. *Semin Nucl Med* 2017; **47**: 5–17. https://doi.org/10.1053/j.semnuclmed.2016.09.004
101. Manabe O, Hattori N, Yamaguchi S, Hirata K, Kobayashi K, Terasaka S, et al. Oligodendroglial component complicates the prediction of tumour grading with metabolic imaging. *Eur J Nucl Med Mol Imaging* 2015; **42**: 896–904. https://doi.org/10.1007/s00259-015-2996-7
102. Valentini MC, Mellai M, Annovazzi L, Melcarne A, Denysenko T, Cassoni P, et al. Comparison among conventional and advanced MRI, ^{18}F-FDG PET/CT, phenotype and genotype in glioblastoma. *Oncotarget* 2017; **8**: 53: 91636–53: . https://doi.org/10.18632/oncotarget.21482
103. Makino K, Hirai T, Nakamura H, Murakami R, Kitajima M, Shigematsu Y, et al. Does adding FDG-PET to MRI improve the differentiation between primary cerebral lymphoma and glioblastoma? observer performance study. *Ann Nucl Med* 2011; **25**: 432–38. https://doi.org/10.1007/s12149-011-0483-1
104. Nakajima S, Okada T, Yamamoto A, Kanagaki M, Fushimi Y, Okada T, et al. Primary central nervous system lymphoma and glioblastoma: differentiation using dynamic susceptibility-contrast perfusion-weighted imaging, diffusion-weighted imaging, and (18)F-fluorodeoxyglucose positron emission tomography. *Clin Imaging* 2015; **39**: 390–95. https://doi.org/10.1016/j.clinimag.2014.12.002
105. Yamashita K, Hiwatashi A, Togao O, Kikuchi K, Kitamura Y, Mizoguchi M, et al. Diagnostic utility of intravoxel incoherent motion mr imaging in differentiating primary central nervous system lymphoma from glioblastoma multiforme. *J Magn Reson Imaging* 2016; **44**: 1256–61. https://doi.org/10.1002/jmri.25261
106. Zou Y, Tong J, Leng H, Jiang J, Pan M, Chen Z. Diagnostic value of using 18F-FDG PET and PET/CT in immunocompetent patients with primary central nervous system lymphoma: A systematic review and meta-analysis. *Oncotarget* 2017; **8**: 41518–28. https://doi.org/10.18632/oncotarget.17456
107. Kosaka N, Tsuchida T, Uematsu H, Kimura H, Okazawa H, Itoh H. 18F-FDG PET of common enhancing malignant brain tumors. *AJR Am J Roentgenol* 2008; **190**: W365–9. https://doi.org/10.2214/AJR.07.2660
108. Makino K, Hirai T, Nakamura H, Murakami R, Kitajima M, Shigematsu Y, et al. Does adding FDG-PET to MRI improve the differentiation between primary cerebral lymphoma and glioblastoma? observer performance study. *Ann Nucl Med* 2011; **25**: 432–38. https://doi.org/10.1007/s12149-011-0483-1
109. Nakajima S, Okada T, Yamamoto A, Kanagaki M, Fushimi Y, Okada T, et al. Primary central nervous system lymphoma and glioblastoma: differentiation using dynamic susceptibility-contrast perfusion-weighted imaging, diffusion-weighted imaging, and 18f-fluorodeoxyglucose positron emission tomography. *Clinical Imaging* 2015; **39**: 390–95. https://doi.org/10.1016/j.clinimag.2014.12.002
110. Iagaru A, Mosci C, Mittra E, Zaharchuk G, Fischbein N, Harsh G, et al. Glioblastoma multiforme recurrence: an exploratory study of (18)f FPPRGD2 PET/CT. *Radiology* 2015; **277**: 497–506. https://doi.org/10.1148/radiol.2015141550
111. Seligman L, Kovanlikaya I, Pisapia DJ, Naeger DM, Magge R, Fine HA, et al. Integrated PET-MRI for glioma surveillance: perfusion-metabolism discordance rate and association with molecular profiling. *AJR Am J Roentgenol* 2019; **212**: 883–91. https://doi.org/10.2214/AJR.18.20531
112. Hatzoglou V, Yang TJ, Omuro A, Gavrilovic I, Ulaner G, Rubel J, et al. A prospective trial of dynamic contrast-enhanced MRI perfusion and fluorine-18 FDG PET-CT in differentiating brain tumor progression from radiation injury after cranial irradiation. *Neuro Oncol* 2016; **18**: 873–80. https://doi.org/10.1093/neuonc/nov301
113. Kim YH, Oh SW, Lim YJ, Park C-K, Lee S-H, Kang KW, et al. Differentiating radiation necrosis from tumor recurrence in high-grade gliomas: assessing the efficacy of 18f-FDG PET, 11c-methionine PET and perfusion MRI. *Clin Neurol Neurosurg* 2010; **112**: 758–65. https://doi.org/10.1016/j.clineuro.2010.06.005
114. Prat R, Galeano I, Lucas A, Martínez JC, Martín M, Amador R, et al. Relative value of magnetic resonance spectroscopy, magnetic resonance perfusion, and 2-(18f) fluoro-2-deoxy-D-glucose positron emission tomography for detection of recurrence or grade increase in gliomas. *J Clin Neurosci* 2010; **17**: 50–53. https://doi.org/10.1016/j.jocn.2009.02.035
115. Hojjati M, Badve C, Garg V, Tatsuoka C, Rogers L, Sloan A, et al. Role of FDG-PET/MRI, FDG-PET/CT, and dynamic susceptibility contrast perfusion MRI in differentiating radiation necrosis from tumor recurrence in glioblastomas. *J Neuroimaging* 2018; **28**: 118–25. https://doi.org/10.1111/jon.12460
116. Jena A, Taneja S, Jha A, Damesha NK, Negi P, Jadhav GK, et al. Multiparametric evaluation in differentiating glioma recurrence from treatment-induced necrosis using simultaneous ^{18}F-FDG-PET/MRI: A single-institution retrospective study. *AJNR Am J Neuroradiol* 2017; **38**: 899–907. https://doi.org/10.3174/ajnr.A5124
117. Lundemann M, Munck Af Rosenschöld P, Muhic A, Larsen VA, Poulsen HS, Engelholm S-A, et al. Feasibility of multi-parametric PET and MRI for prediction of tumour recurrence in patients with glioblastoma. *Eur J Nucl Med Mol Imaging* 2019; **46**: 603–13. https://doi.org/10.1007/s00259-018-4180-3
118. Ozsunar Y, Mullins ME, Kwong K, Hochberg FH, Ament C, Schaefer PW, et al. Glioma recurrence versus radiation necrosis? A pilot comparison of arterial spin-labeled, dynamic susceptibility contrast enhanced MRI, and FDG-PET imaging. *Acad Radiol* 2010; **17**: 282–90. https://doi.org/10.1016/j.acra.2009.10.024
119. Cui M, Zorrilla-Veloz RI, Hu J, Guan B, Ma X. Diagnostic accuracy of PET for differentiating true glioma progression from post treatment-related changes: A systematic review and meta-analysis. *Front Neurol* 2021; **12**: 671867. https://doi.org/10.3389/fneur.2021.671867
120. Rapp M, Heinzel A, Galldiks N, Stoffels G, Felsberg J, Ewelt C, et al. diagnostic performance of ^{18} f-FET PET in newly diagnosed cerebral lesions suggestive of glioma . *J Nucl Med* 2013; **54**: 229–35. https://doi.org/10.2967/jnumed.112.109603
121. Hutterer M, Nowosielski M, Putzer D, Jansen NL, Seiz M, Schocke M, et al. [18F]-fluoro-ethyl-L-tyrosine PET: a valuable diagnostic tool in neuro-oncology, but not all that glitters is glioma. *Neuro-Oncology* 2013; **15**: 341–51. https://doi.org/10.1093/neuonc/nos300
122. Jansen NL, Suchorska B, Wenter V, Schmid-Tannwald C, Todica A, Eigenbrod S, et al. prognostic significance of dynamic ^{18} f-FET PET in newly diagnosed astrocytic high-grade glioma . *J Nucl Med* 2013; **56**: 9–15. https://doi.org/10.2967/jnumed.114.144675
123. Pöpperl G, Kreth FW, Mehrkens JH, Herms J, Seelos K, Koch W, et al. FET PET for the evaluation of untreated gliomas: correlation of FET uptake and uptake kinetics with tumour grading. *Eur J Nucl Med Mol Imaging* 2013; **34**: 1933–42. https://doi.org/10.1007/s00259-007-0534-y

124. Lohmann P, Herzog H, Rota Kops E, Stoffels G, Judov N, Filss C, et al. Dual-time-point O-(2-[18f]fluoroethyl)-L-tyrosine PET for grading of cerebral gliomas. *Eur Radiol* 2013; **25**: 3017–24. https://doi.org/10.1007/s00330-015-3691-6
125. Dunet V, Maeder P, Nicod-Lalonde M, Lhermitte B, Pollo C, Bloch J, et al. Combination of MRI and dynamic FET PET for initial glioma grading. *Nuklearmedizin* 2014; **53**: 155–61. https://doi.org/10.3413/Nukmed-0650-14-03
126. Moulin-Romsée G, D'Hondt E, de Groot T, Goffin J, Sciot R, Mortelmans L, et al. Non-invasive grading of brain tumours using dynamic amino acid PET imaging: does it work for 11C-methionine? *Eur J Nucl Med Mol Imaging* 2007; **34**: 2082–87. https://doi.org/10.1007/s00259-007-0557-4
127. Kratochwil C, Combs SE, Leotta K, Afshar-Oromieh A, Rieken S, Debus J, et al. Intra-individualcomparison of (1)(8)F-FET and (1)(8)F-DOPA in PET imaging of recurrent brain tumors. *Neuro Oncol* 2014; **16**: 434–40. https://doi.org/10.1093/neuonc/not199
128. Schiepers C, Chen W, Cloughesy T, Dahlbom M, Huang SC. 18F-FDOPA kinetics in brain tumors. *J Nucl Med* 2007; **48**: 1651–61. https://doi.org/10.2967/jnumed.106.039321
129. Pauleit D, Floeth F, Hamacher K, Riemenschneider MJ, Reifenberger G, Müller H-W, et al. O-(2-[18F]fluoroethyl)-L-tyrosine PET combined with MRI improves the diagnostic assessment of cerebral gliomas. *Brain* 2005; **128**: 678–87. https://doi.org/10.1093/brain/awh399
130. Lopez WOC, Cordeiro JG, Albicker U, Doostkam S, Nikkhah G, Kirch RD, et al. Correlation of (18)F-fluoroethyl tyrosine positron-emission tomography uptake values and histomorphological findings by stereotactic serial biopsy in newly diagnosed brain tumors using a refined software tool. *Onco Targets Ther* 2015; **8**: 3803–15. https://doi.org/10.2147/OTT.S87126
131. Filss CP, Galldiks N, Stoffels G, Sabel M, Wittsack HJ, Turowski B, et al. Comparison of 18F-FET PET and perfusion-weighted MR imaging: a PET/MR imaging hybrid study in patients with brain tumors. *J Nucl Med* 2014; **55**: 540–45. https://doi.org/10.2967/jnumed.113.129007
132. Cicone F, Filss CP, Minniti G, Rossi-Espagnet C, Papa A, Scaringi C, et al. Volumetric assessment of recurrent or progressive gliomas: comparison between F-DOPA PET and perfusion-weighted MRI. *Eur J Nucl Med Mol Imaging* 2015; **42**: 905–15. https://doi.org/10.1007/s00259-015-3018-5
133. Pafundi DH, Laack NN, Youland RS, Parney IF, Lowe VJ, Giannini C, et al. Biopsy validation of 18F-DOPA PET and biodistribution in gliomas for neurosurgical planning and radiotherapy target delineation: results of a prospective pilot study. *Neuro Oncol* 2013; **15**: 1058–67. https://doi.org/10.1093/neuonc/not002
134. Kosztyla R, Chan EK, Hsu F, Wilson D, Ma R, Cheung A, et al. High-grade glioma radiation therapy target volumes and patterns of failure obtained from magnetic resonance imaging and 18F-FDOPA positron emission tomography delineations from multiple observers. *Int J Radiat Oncol Biol Phys* 2013; **87**: 1100–1106. https://doi.org/10.1016/j.ijrobp.2013.09.008
135. Galldiks N, Ullrich R, Schroeter M, Fink GR, Jacobs AH, Kracht LW. Volumetry of [(11)c]-methionine pet uptake and mri contrast enhancement in patients with recurrent glioblastoma multiforme. *Eur J Nucl Med Mol Imaging* 2010; **37**: 84–92. https://doi.org/10.1007/s00259-009-1219-5
136. Harris RJ, Cloughesy TF, Pope WB, Nghiemphu PL, Lai A, Zaw T, et al. 18F-FDOPA and 18F-FLT positron emission tomography parametric response maps predict response in recurrent malignant gliomas treated with bevacizumab. *Neuro Oncol* 2012; **14**: 1079–89. https://doi.org/10.1093/neuonc/nos141
137. Schwarzenberg J, Czernin J, Cloughesy TF, Ellingson BM, Pope WB, Grogan T, et al. Treatment response evaluation using 18F-FDOPA PET in patients with recurrent malignant glioma on bevacizumab therapy. *Clin Cancer Res* 2014; **20**: 3550–59. https://doi.org/10.1158/1078-0432.CCR-13-1440
138. Pirotte B, Goldman S, Brucher JM, Zomosa G, Baleriaux D, Brotchi J, et al. PET in stereotactic conditions increases the diagnostic yield of brain biopsy. *Stereotact Funct Neurosurg* 1994; **63**: 144–49. https://doi.org/10.1159/000100306
139. Lindberg OR, McKinney A, Engler JR, Koshkakaryan G, Gong H, Robinson AE, et al. GBM heterogeneity as a function of variable epidermal growth factor receptor variant III activity. *Oncotarget* 2016; **7**: 79101–16. https://doi.org/10.18632/oncotarget.12600
140. Pirotte B, Goldman S, Massager N, David P, Wikler D, Vandesteene A, et al. Comparison of 18F-FDG and 11C-methionine for PET-guided stereotactic brain biopsy of gliomas. *J Nucl Med* 2004; **45**: 1293–98.
141. Furtak J, Rakowska J, Szylberg T, Harat M, Małkowski B, Harat M. Glioma biopsy based on hybrid dual time-point FET-PET/MRI-A proof of concept study. *Front Neurol* 2021; **12**: 634609. https://doi.org/10.3389/fneur.2021.634609
142. Heinzel A, Stock S, Langen K-J, Müller D. Cost-effectiveness analysis of FET PET-guided target selection for the diagnosis of gliomas. *Eur J Nucl Med Mol Imaging* 2012; **39**: 1089–96. https://doi.org/10.1007/s00259-012-2093-0
143. Navarria P, Reggiori G, Pessina F, Ascolese AM, Tomatis S, Mancosu P, et al. Investigation on the role of integrated PET/MRI for target volume definition and radiotherapy planning in patients with high grade glioma. *Radiother Oncol* 2014; **112**: 425–29. https://doi.org/10.1016/j.radonc.2014.09.004
144. Lee IH, Piert M, Gomez-Hassan D, Junck L, Rogers L, Hayman J, et al. Association of 11C-methionine PET uptake with site of failure after concurrent temozolomide and radiation for primary glioblastoma multiforme. *Int J Radiat Oncol Biol Phys* 2009; **73**: 479–85. https://doi.org/10.1016/j.ijrobp.2008.04.050
145. Grosu AL, Weber WA, Riedel E, Jeremic B, Nieder C, Franz M, et al. L-(methyl-11C) methionine positron emission tomography for target delineation in resected high-grade gliomas before radiotherapy. *Int J Radiat Oncol Biol Phys* 2005; **63**: 64–74.
146. Munck Af Rosenschold P, Costa J, Engelholm SA, Lundemann MJ, Law I, Ohlhues L, et al. Impact of [18f]-fluoro-ethyl-tyrosine PET imaging on target definition for radiation therapy of high-grade glioma. *Neuro Oncol* 2015; **17**: 757–63. https://doi.org/10.1093/neuonc/nou316
147. Rieken S, Habermehl D, Giesel FL, Hoffmann C, Burger U, Rief H, et al. Analysis of FET-PET imaging for target volume definition in patients with gliomas treated with conformal radiotherapy. *Radiother Oncol* 2013; **109**: 487–92. https://doi.org/10.1016/j.radonc.2013.06.043
148. Piroth MD, Galldiks N, Pinkawa M, Holy R, Stoffels G, Ermert J, et al. Relapse patterns after radiochemotherapy of glioblastoma with FET PET-guided boost irradiation and simulation to optimize radiation target volume. *Radiat Oncol* 2016; **11**. https://doi.org/10.1186/s13014-016-0665-z
149. Lundemann M, Costa JC, Law I, Engelholm SA, Muhic A, Poulsen HS, et al. Patterns of failure for patients with glioblastoma following 0-(2-[F-18] fluoroethyl)-L-tyrosine PET- and MRI-guided radiotherapy. *Radiother Oncol* 2017; **122**: 380–86.
150. Takenaka S, Asano Y, Shinoda J, Nomura Y, Yonezawa S, Miwa K, et al. Comparison

of (11)C-methionine, (11)C-choline, and (18)F-fluorodeoxyglucose-PET for distinguishing glioma recurrence from radiation necrosis. *Neurol Med Chir (Tokyo)* 2014; **54**: 280–89. https://doi.org/10.2176/nmc.oa2013-0117

151. Kim YH, Oh SW, Lim YJ, Park C-K, Lee S-H, Kang KW, et al. Differentiating radiation necrosis from tumor recurrence in high-grade gliomas: assessing the efficacy of 18F-FDG PET, 11C-methionine PET and perfusion MRI. *Clin Neurol Neurosurg* 2010; **112**: 758–65. https://doi.org/10.1016/j.clineuro.2010.06.005
152. Deuschl C, Kirchner J, Poeppel TD, Schaarschmidt B, Kebir S, El Hindy N, et al. 11C–MET PET/MRI for detection of recurrent glioma. *Eur J Nucl Med Mol Imaging* 2018; **45**: 593–601. https://doi.org/10.1007/s00259-017-3916-9
153. Minamimoto R, Saginoya T, Kondo C, Tomura N, Ito K, Matsuo Y, et al. Differentiation of brain tumor recurrence from post-radiotherapy necrosis with 11C-methionine PET: visual assessment versus quantitative assessment. *PLoS One* 2015; **10**(7): e0132515. https://doi.org/10.1371/journal.pone.0132515
154. Okamoto S, Shiga T, Hattori N, Kubo N, Takei T, Katoh N, et al. Semiquantitative analysis of C-11 methionine PET may distinguish brain tumor recurrence from radiation necrosis even in small lesions. *Ann Nucl Med* 2011; **25**: 213–20. https://doi.org/10.1007/s12149-010-0450-2
155. Tomura N, Kokubun M, Saginoya T, Mizuno Y, Kikuchi Y. Differentiation between treatment-induced necrosis and recurrent tumors in patients with metastatic brain tumors: comparison among ^{11}C-methionine-PET, FDG-PET, MR permeability imaging, and MRI-ADC-preliminary results. *AJNR Am J Neuroradiol* 2017; **38**: 1520–27. https://doi.org/10.3174/ajnr.A5252
156. Terakawa Y, Tsuyuguchi N, Iwai Y, Yamanaka K, Higashiyama S, Takami T, et al. Diagnostic accuracy of 11C-methionine PET for differentiation of recurrent brain tumors from radiation necrosis after radiotherapy. *J Nucl Med* 2008; **49**: 694–99. https://doi.org/10.2967/jnumed.107.048082
157. Dandois V, Rommel D, Renard L, Jamart J, Cosnard G. Substitution of 11C-methionine PET by perfusion MRI during the follow-up of treated high-grade gliomas: preliminary results in clinical practice. *J Neuroradiol* 2010; **37**: 89–97. https://doi.org/10.1016/j.neurad.2009.04.005
158. Qiao Z, Zhao X, Wang K, Zhang Y, Fan D, Yu T, et al. Utility of dynamic susceptibility contrast perfusion-weighted MR imaging and ^{11}C-methionine PET/CT for differentiation of tumor recurrence from radiation injury in patients with high-grade gliomas. *AJNR Am J Neuroradiol* 2019; **40**: 253–59. https://doi.org/10.3174/ajnr.A5952
159. Kim YH, Oh SW, Lim YJ, Park C-K, Lee S-H, Kang KW, et al. Differentiating radiation necrosis from tumor recurrence in high-grade gliomas: assessing the efficacy of 18F-FDG PET, 11C-methionine PET and perfusion MRI. *Clin Neurol Neurosurg* 2010; **112**: 758–65. https://doi.org/10.1016/j.clineuro.2010.06.005
160. Steidl E, Langen K-J, Hmeidan SA, Polomac N, Filss CP, Galldiks N, et al. Sequential implementation of dsc-mr perfusion and dynamic [^{18}f]fet pet allows efficient differentiation of glioma progression from treatment-related changes. *Eur J Nucl Med Mol Imaging* 2021; **48**: 1956–65. https://doi.org/10.1007/s00259-020-05114-0
161. Clement P, Smits M, van Osch MJP, Costa BM, Warnert EAH. Micro- to macroscale magnetic resonance imaging of glioma. *MAGMA* 2022; **35**: 1–2. https://doi.org/10.1007/s10334-021-00999-w
162. Galldiks N, Stoffels G, Filss C, Rapp M, Blau T, Tscherpel C, et al. The use of dynamic O-(2-18F-fluoroethyl)-l-tyrosine PET in the diagnosis of patients with progressive and recurrent glioma. *Neuro Oncol* 2015; **17**: 1293–1300. https://doi.org/10.1093/neuonc/nov088
163. Jena A, Taneja S, Gambhir A, Mishra AK, D'souza MM, Verma SM, et al. Glioma recurrence versus radiation necrosis: single-session multiparametric approach using simultaneous O-(2-18F-fluoroethyl)-L-tyrosine PET/MRI. *Clin Nucl Med* 2016; **41**: e228–36. https://doi.org/10.1097/RLU.0000000000001152
164. Pyka T, Hiob D, Preibisch C, Gempt J, Wiestler B, Schlegel J, et al. Diagnosis of glioma recurrence using multiparametric dynamic 18F-fluoroethyl-tyrosine PET-MRI. *Eur J Radiol* 2018; **103**: 32–37. https://doi.org/10.1016/j.ejrad.2018.04.003
165. Sogani SK, Jena A, Taneja S, Gambhir A, Mishra AK, D'Souza MM, et al. Potential for differentiation of glioma recurrence from radionecrosis using integrated ^{18}F-fluoroethyl-L-tyrosine (FET) positron emission tomography/magnetic resonance imaging: A prospective evaluation. *Neurol India* 2017; **65**: 293–301. https://doi.org/10.4103/neuroindia.NI_101_16
166. Verger A, Filss CP, Lohmann P, Stoffels G, Sabel M, Wittsack H-J, et al. Comparison of O-(2-^{18}f-fluoroethyl)-L-tyrosine positron emission tomography and perfusion-weighted magnetic resonance imaging in the diagnosis of patients with progressive and recurrent glioma: A hybrid positron emission tomography/magnetic resonance study. *World Neurosurg* 2018; **113**: e727–37. https://doi.org/10.1016/j.wneu.2018.02.139
167. Furuse M, Nonoguchi N, Yamada K, Shiga T, Combes J-D, Ikeda N, et al. Radiological diagnosis of brain radiation necrosis after cranial irradiation for brain tumor: a systematic review. *Radiat Oncol* 2019; **14**: 28. https://doi.org/10.1186/s13014-019-1228-x
168. Yu J, Zheng J, Xu W, Weng J, Gao L, Tao L, et al. Accuracy of ^{18}f-FDOPA positron emission tomography and ^{18}f-FET positron emission tomography for differentiating radiation necrosis from brain tumor recurrence. *World Neurosurg* 2018; **114**: e1211–24. https://doi.org/10.1016/j.wneu.2018.03.179
169. Fraioli F, Shankar A, Hyare H, Ferrazzoli V, Militano V, Samandouras G, et al. The use of multiparametric 18F-fluoro-L-3,4-dihydroxy-phenylalanine PET/MRI in post-therapy assessment of patients with gliomas. *Nucl Med Commun* 2020; **41**: 517–25. https://doi.org/10.1097/MNM.0000000000001184
170. Pellerin A, Khalifé M, Sanson M, Rozenblum-Beddok L, Bertaux M, Soret M, et al. Simultaneously acquired PET and ASL imaging biomarkers may be helpful in differentiating progression from pseudo-progression in treated gliomas. *Eur Radiol* 2021; **31**: 7395–7405. https://doi.org/10.1007/s00330-021-07732-0
171. Karunanithi S, Sharma P, Kumar A, Khangembam BC, Bandopadhyaya GP, Kumar R, et al. 18F-FDOPA PET/CT for detection of recurrence in patients with glioma: prospective comparison with 18F-FDG PET/CT. *Eur J Nucl Med Mol Imaging* 2013; **40**: 1025–35. https://doi.org/10.1007/s00259-013-2384-0
172. Clement P, Booth T, Borovečki F, Emblem KE, Figueiredo P, Hirschler L, et al. GliMR: cross-border collaborations to promote advanced MRI biomarkers for glioma. *J Med Biol Eng* 2021; **41**: 115–25. https://doi.org/10.1007/s40846-020-00582-z
173. Jensen JH, Helpern JA, Ramani A, Lu HZ, Kaczynski K. Diffusional kurtosis imaging: the quantification of non-gaussian water diffusion by means of magnetic resonance imaging. *Magn Reson Med* 2005; **53**: 1432–40. https://doi.org/10.1002/mrm.20508
174. Delgado AF, Fahlström M, Nilsson M, Berntsson SG, Zetterling M, Libard S, et al. Diffusion kurtosis imaging of gliomas

grades II and III - a study of perilesional tumor infiltration, tumor grades and subtypes at clinical presentation. *Radiol Oncol* 2017; **51**: 121–29. https://doi.org/10.1515/raon-2017-0010
175. Qiu J, Deng K, Wang P, Chen C, Luo Y, Yuan S, et al. Application of diffusion kurtosis imaging to the study of edema in solid and peritumoral areas of glioma. *Magn Reson Imaging* 2022; **86**: 10–16. https://doi.org/10.1016/j.mri.2021.11.001
176. Paech D, Windschuh J, Oberhollenzer J, Dreher C, Sahm F, Meissner J-E, et al. Assessing the predictability of IDH mutation and MGMT methylation status in glioma patients using relaxation-compensated multipool CEST MRI at 7.0 T. *Neuro Oncol* 2018; **20**: 1661–71. https://doi.org/10.1093/neuonc/noy073
177. Chan RW, Chen H, Myrehaug S, Atenafu EG, Stanisz GJ, Stewart J, et al. Quantitative CEST and MT at 1.5T for monitoring treatment response in glioblastoma: early and late tumor progression during chemoradiation. *J Neurooncol* 2021; **151**: 267–78. https://doi.org/10.1007/s11060-020-03661-y
178. Meissner J-E, Korzowski A, Regnery S, Goerke S, Breitling J, Floca RO, et al. Early response assessment of glioma patients to definitive chemoradiotherapy using chemical exchange saturation transfer imaging at 7 T. *J Magn Reson Imaging* 2019; **50**: 1268–77. https://doi.org/10.1002/jmri.26702
179. De Feyter HM, Behar KL, Corbin ZA, Fulbright RK, Brown PB, McIntyre S, et al. Deuterium metabolic imaging (DMI) for MRI-based 3D mapping of metabolism in vivo. *Sci Adv* 2018; **4**: eaat7314. https://doi.org/10.1126/sciadv.aat7314
180. Dennie J, Mandeville JB, Boxerman JL, Packard SD, Rosen BR, Weisskoff RM. NMR imaging of changes in vascular morphology due to tumor angiogenesis. *Magn Reson Med* 1998; **40**: 793–99. https://doi.org/10.1002/mrm.1910400602
181. Chakhoyan A, Yao J, Leu K, Pope WB, Salamon N, Yong W, et al. Validation of vessel size imaging (VSI) in high-grade human gliomas using magnetic resonance imaging, image-guided biopsies, and quantitative immunohistochemistry. *Sci Rep* 2019; **9**(1): 2846. https://doi.org/10.1038/s41598-018-37564-w
182. Kiselev VG, Strecker R, Ziyeh S, Speck O, Hennig J. Vessel size imaging in humans. *Magn Reson Med* 2005; **53**: 553–63. https://doi.org/10.1002/mrm.20383
183. Kim M, Park JE, Emblem K, Bjørnerud A, Kim HS. Vessel type determined by vessel architectural imaging improves differentiation between early tumor progression and pseudoprogression in glioblastoma. *AJNR Am J Neuroradiol* 2021; **42**: 663–70. https://doi.org/10.3174/ajnr.A6984
184. Emblem KE, Mouridsen K, Bjornerud A, Farrar CT, Jennings D, Borra RJH, et al. Vessel architectural imaging identifies cancer patient responders to anti-angiogenic therapy. *Nat Med* 2013; **19**: 1178–83. https://doi.org/10.1038/nm.3289
185. Traub-Weidinger T, Poetsch N, Woehrer A, Klebermass E-M, Bachnik T, Preusser M, et al. PSMA expression in 122 treatment naive glioma patients related to tumor metabolism in ^{11}C-methionine PET and survival. *J Pers Med* 2021; **11**(7): 624. https://doi.org/10.3390/jpm11070624
186. Holzgreve A, Biczok A, Ruf VC, Liesche-Starnecker F, Steiger K, Kirchner MA, et al. PSMA expression in glioblastoma as A basis for theranostic approaches: A retrospective, correlational panel study including immunohistochemistry, clinical parameters and PET imaging. *Front Oncol* 2021; **11**: 646387. https://doi.org/10.3389/fonc.2021.646387
187. Kumar A, ArunRaj ST, Bhullar K, Haresh KP, Gupta S, Ballal S, et al. Ga-68 PSMA PET/CT in recurrent high-grade gliomas: evaluating PSMA expression in vivo. *Neuroradiology* 2022; **64**: 969–79. https://doi.org/10.1007/s00234-021-02828-2
188. Kunikowska J, Kuliński R, Muylle K, Koziara H, Królicki L. 68Ga-prostate-specific membrane antigen-11 PET/CT: A new imaging option for recurrent glioblastoma multiforme? *Clin Nucl Med* 2020; **45**: 11–18.
189. Giesel FL, Kratochwil C, Lindner T, Marschalek MM, Loktev A, Lehnert W, et al. 68)ga-FAPI PET/CT: biodistribution and preliminary dosimetry estimate of 2 DOTA-containing FAP-targeting agents in patients with various cancers. *J Nucl Med* 2019; **60**: 386–92.
190. van Leeuwen KG, Schalekamp S, Rutten MJCM, van Ginneken B, de Rooij M. Artificial intelligence in radiology: 100 commercially available products and their scientific evidence. *Eur Radiol* 2021; **31**: 3797–3804. https://doi.org/10.1007/s00330-021-07892-z
191. van der Voort SR, Incekara F, Wijnenga MMJ, Kapas G, Gardeniers M, Schouten JW, et al. Predicting the 1p/19q codeletion status of presumed low-grade glioma with an externally validated machine learning algorithm. *Clin Cancer Res* 2019; **25**: 7455–62. https://doi.org/10.1158/1078-0432.CCR-19-1127
192. Abdel Razek AAK, Alksas A, Shehata M, AbdelKhalek A, Abdel Baky K, El-Baz A, et al. Clinical applications of artificial intelligence and radiomics in neuro-oncology imaging. *Insights Imaging* 2021; **12**(1): 152. https://doi.org/10.1186/s13244-021-01102-6
193. Menze BH, Jakab A, Bauer S, Kalpathy-Cramer J, Farahani K, Kirby J, et al. The multimodal brain tumor image segmentation benchmark (BRATS). *IEEE Trans Med Imaging* 2015; **34**: 1993–2024. https://doi.org/10.1109/TMI.2014.2377694
194. van der Voort SR, Incekara F, Wijnenga MMJ, Kapsas G, Gahrmann R, Schouten JW, et al. The erasmus glioma database (EGD): structural MRI scans, WHO 2016 subtypes, and segmentations of 774 patients with glioma. *Data Brief* 2021; **37**: 107191. https://doi.org/10.1016/j.dib.2021.107191
195. van der Voort SR, Smits M, Klein S, Alzheimer's Disease Neuroimaging Initiative. DeepDicomSort: an automatic sorting algorithm for brain magnetic resonance imaging data. *Neuroinformatics* 2021; **19**: 159–84. https://doi.org/10.1007/s12021-020-09475-7
196. van Kempen EJ, Post M, Mannil M, Witkam RL, Ter Laan M, Patel A, et al. Performance of machine learning algorithms for glioma segmentation of brain MRI: a systematic literature review and meta-analysis. *Eur Radiol* 2021; **31**: 9638–53. https://doi.org/10.1007/s00330-021-08035-0
197. van Garderen KA, van der Voort SR, Versteeg A, Koek M, Gutierrez A, van Straten M, et al. EASE: clinical implementation of automated tumor segmentation and volume quantification for adult low-grade glioma. *Front Med* 2021; **8**: 1791. https://doi.org/10.3389/fmed.2021.738425
198. De Looze C, Beausang A, Cryan J, Loftus T, Buckley PG, Farrell M, et al. Machine learning: a useful radiological adjunct in determination of a newly diagnosed glioma's grade and IDH status. *J Neurooncol* 2018; **139**: 491–99. https://doi.org/10.1007/s11060-018-2895-4
199. van Kempen EJ, Post M, Mannil M, Kusters B, ter Laan M, Meijer FJA, et al. (n.d.). Accuracy of machine learning algorithms for the classification of molecular features of gliomas on MRI: A systematic literature review and meta-analysis. *Cancers*; **13**: 2606. https://doi.org/10.3390/cancers13112606
200. Jian A, Jang K, Manuguerra M, Liu S, Magnussen J, Di Ieva A. Machine learning for the prediction of molecular markers in glioma on magnetic resonance imaging: A systematic review and meta-analysis.

Neurosurgery 2021; **89**: 31–44. https://doi.org/10.1093/neuros/nyab103

201. Manfrini E, Smits M, Thust S, Geiger S, Bendella Z, Petr J, et al. From research to clinical practice: a european neuroradiological survey on quantitative advanced MRI implementation. *Eur Radiol* 2021; **31**: 6334–41. https://doi.org/10.1007/s00330-020-07582-2
202. Boxerman JL, Quarles CC, Hu LS, Erickson BJ, Gerstner ER, Smits M, et al. Consensus recommendations for a dynamic susceptibility contrast MRI protocol for use in high-grade gliomas. *Neuro Oncol* 2020; **22**: 1262–75. https://doi.org/10.1093/neuonc/noaa141
203. Lambin P, Leijenaar RTH, Deist TM, Peerlings J, de Jong EEC, van Timmeren J, et al. Radiomics: the bridge between medical imaging and personalized medicine. *Nat Rev Clin Oncol* 2017; **14**: 749–62. https://doi.org/10.1038/nrclinonc.2017.141